NASA/TM–2020-220575

Bi-Axial Load Testing of a Woven-Webbing Inflatable Space Habitat Restraint Layer Component

Karen H. Lyle and Thomas C. Jones
Langley Research Center, Hampton, Virginia

March 2020

NASA STI Program . . . in Profile

Since its founding, NASA has been dedicated to the advancement of aeronautics and space science. The NASA scientific and technical information (STI) program plays a key part in helping NASA maintain this important role.

The NASA STI program operates under the auspices of the Agency Chief Information Officer. It collects, organizes, provides for archiving, and disseminates NASA's STI. The NASA STI program provides access to the NTRS Registered and its public interface, the NASA Technical Reports Server, thus providing one of the largest collections of aeronautical and space science STI in the world. Results are published in both non-NASA channels and by NASA in the NASA STI Report Series, which includes the following report types:

- TECHNICAL PUBLICATION. Reports of completed research or a major significant phase of research that present the results of NASA Programs and include extensive data or theoretical analysis. Includes compilations of significant scientific and technical data and information deemed to be of continuing reference value. NASA counter-part of peer-reviewed formal professional papers but has less stringent limitations on manuscript length and extent of graphic presentations.

- TECHNICAL MEMORANDUM. Scientific and technical findings that are preliminary or of specialized interest, e.g., quick release reports, working papers, and bibliographies that contain minimal annotation. Does not contain extensive analysis.

- CONTRACTOR REPORT. Scientific and technical findings by NASA-sponsored contractors and grantees.

- CONFERENCE PUBLICATION. Collected papers from scientific and technical conferences, symposia, seminars, or other meetings sponsored or co-sponsored by NASA.

- SPECIAL PUBLICATION. Scientific, technical, or historical information from NASA programs, projects, and missions, often concerned with subjects having substantial public interest.

- TECHNICAL TRANSLATION. English-language translations of foreign scientific and technical material pertinent to NASA's mission.

Specialized services also include organizing and publishing research results, distributing specialized research announcements and feeds, providing information desk and personal search support, and enabling data exchange services.

For more information about the NASA STI program, see the following:

- Access the NASA STI program home page at http://www.sti.nasa.gov

- E-mail your question to help@sti.nasa.gov

- Phone the NASA STI Information Desk at 757-864-9658

- Write to:
  NASA STI Information Desk
  Mail Stop 148
  NASA Langley Research Center
  Hampton, VA 23681-2199

NASA/TM–2020-220575

Bi-Axial Load Testing of a Woven-Webbing Inflatable Space Habitat Restraint Layer Component

Karen H. Lyle and Thomas C. Jones
Langley Research Center, Hampton, Virginia

National Aeronautics and
Space Administration

Langley Research Center
Hampton, Virginia 23681-2199

March 2020

Available from:

NASA STI Program / Mail Stop 148
NASA Langley Research Center
Hampton, VA 23681-2199
Fax: 757-864-6500

Abstract

This report discusses testing of a bi-axial woven panel consisting of high-strength webbings that represent a portion of the structural restraint layer of an inflatable space structure. Inflatable softgoods vessels are being researched for human space missions as possible habitats, airlocks and tunnel elements. Understanding the complex behavior of the softgoods restraint layer and maturing finite element analysis capabilities to model these structures is critical to their successful implementation. The primary goal of this research is to study the load-up and load distribution in a weave of webbings, before and after the loss of tension in one of the webbings. In addition, a key objective is to evaluate the ability to convert strains measured via photogrammetry using digital image correlation to loads in the weave. The report gives an introduction and objectives for the test program and a description of the test fixture, setup and procedure. This is followed by a section focusing on the test data and associated discussion. To streamline presentation of the data, one focus case is detailed in the main text. (Comprehensive data set can be found in Appendix A for the three remaining test cases.) In addition to the load and time histories for one case, summary charts and tables that incorporate data from all four test cases are provided. The concluding remarks include major findings, lessons learned and recommendations for future work. Appendix B provides complementary full-field strain results when considering the existing woven webbing data as a fabric. These types of results could inform models intended for global representation. Appendix C contains a description from a series of exploratory instrumented-hammer tap tests and results on the weave. These tests describe an area of research for the bi-axial test fixture beyond the current testing studying the propagation and detection of vibrations in a tensioned weave, that has applications in impact and damage detection.

Nomenclature

- AW = axial webbing (6K Vectran)
- DAQ = data acquisition system
- DIC = digital image correlation
- HW = hoop webbing (12.5K Vectran)
- P = load
- SP = set point
- T = time
- ε = strain
- μ = mean
- σ = standard deviation

Introduction

Inflatable softgoods structures are being researched and developed at NASA and in industry to provide large deployable crewed pressure vessels for space applications including habitats, airlocks and tunnel elements. Their primary advantage over rigid structures is the ability

to package compactly for launch, which enables larger habitable volumes to be deployed at the mission site. In addition, inflatables enable the use of smaller launch vehicles, or the ability to launch multiple habitable elements on a single larger launch vehicle such as NASA's Space Launch System (SLS). These structures consist of multiple flexible layers, as shown in Figure 1(a), that protect the astronauts from micrometeoroid and orbital debris (MMOD) and the extreme thermal environment of space, using multi-layer insulation (MLI). In low earth orbit (LEO) applications, an outer Atomic Oxygen (AO) protection layer is also added to prevent oxidation and erosion. Beneath these, but above the internal redundant air retention (or bladder) layers, the restraint layer provides the tensile structure to the vessel via an architecture of high-strength webbings, cordage and/or fabric, of which there are many different possible designs and variants. The restraint layer is in a relatively benign environment when in service due to its location under the insulation and it is not expected to see large temperature fluctuations or be impacted by direct sunlight.

The restraint layer architecture used for the bi-axial component testing in this study was employed by NASA in several inflatable structure designs, including the TransHab[1] that is shown in Figure 1(b). Transhab is a large habitat conceived of as a primary habitable volume for the International Space Station or a transit mission to Mars. This restraint layer architecture consists of a tight, plain weave of two strengths of Vectran webbings, specifically, 6,000 lbs and 12,500 lbs, see Figure 1(c) and Table I. The 2:1 strength ratio in the weave is due to the stress ratio found in a pressurized cylinder (i.e. the mid-section of the habitat), where the hoop stresses are twice those of the axial stresses. The 6,000-lbs and 12,500-lbs minimum strengths were required for a vessel of the TransHab's 27 ft deployed diameter, with an operational pressure of 14.7 ± 0.5 psig and a safety factor of 4 based on NASA standard requirements[2]. Due to the tight weave, no additional structural fabric is required to fill gaps between the webbings to protect the underlying bladder from herniation.

Understanding the load carrying and load transfer behavior of these webbings in a woven architecture, specifically before and after a single webbing failure, is the focus of this work. This is of interest to determine the load changes in adjacent webbings if a failure occurs, so that a safe life design can include the pertinent knock-down factors. The ability of the load to redistribute around a failed webbing can significantly enhance the robustness of a woven-webbing approach but important aspects concerning the load redistribution capability need to be understood, including: which parameters affect the size and shape of the affected zone; and how to enhance this load redistribution. Prevention of a catastrophic failure and the quantitative understanding of the performance of a woven restraint architecture are critical to an effective and safe design. In addition, evaluating the ability to convert strains, measured via photogrammetry using digital image correlation (DIC), to loads in the weave was a key objective. A low cost bi-axial test fixture was designed and constructed to support this work. The test fixture is described in detail in the next section along with an overview of the test and webbing preparation. A complementary analytical modeling effort is also being pursued to improve NASA's understanding of the behavior and key influence parameters of the woven restraint layer, and to identify deficiencies or gaps in our ability to model a complex softgoods component. To provide the required input data to the model for comparison and correlation with the tests, the bi-axial test fixture is instrumented to measure individual loads at the end interfaces of each webbing in the panel, and strains in the webbings over the entire woven panel via photogrammetry. Prior work on these woven-webbing

structures had focused primarily on individual webbings or entire inflatable modules. The testing described here is considered an important bridge between those two structural levels.

Description of Bi-Axial Fixture

Fixture Design

The bi-axial test fixture design was driven by several factors including: the ability to accurately represent a portion of a softgoods inflatable design; the ability to model the setup, boundary conditions, and test in a finite element model; and the overall cost. In addition, manual control over the tensioning of each webbing was included in the design to allow adjustment of the load distribution at the boundaries. The load distribution at the boundaries could then be compared to observations of the load distribution and evolution within the weave. To reduce the overall cost of the fixture, only a single hydraulic actuator is used to provide automated load control in one direction, nominally the hoop direction. The perpendicular loading is applied by manually tightening nuts at the interfaces of the axial webbings. Photographs of the test setup are provided in Figure 2. Overview schematics of the bi-axial test fixture are provided in Figure 3. Close-up schematics of the load introduction hardware are shown in Figures 4. In addition, the photographs in Figures 4 (b) and (c) show that the webbings were not terminated at the frame in a single plane. Specifically, for the hoop webbings, there were 8 webbings that terminated above the mid-plane and 7 webbings below the mid-plane. This uneven distribution of webbings about the mid-plane was seen to introduce a torque on the frame. Although the torque can be discernable in the webbing loads, it is not considered to significantly affect the results.

Test Fixture Hardware

The 100-Kip hydraulic actuator is fixed to a reaction structure that is bolted to the ground. The hydraulic actuator is also attached to an Interface 1040BF-100Kip load cell and movable load introduction frame on roller bearings that has connection points for up to 15 webbings. The perpendicular set of up to 9 webbings are attached to a floating, self-reacting frame, also on roller bearings that allows the perpendicular webbings to move in the actuation direction freely (i.e. travel in a rigid body sense as the actuator is moved) while still allowing for load to be applied to those webbings using the load introduction hardware. The pattern plates, shown in green in Figure 4, establish the webbing spacing which can be different in axial and hoop directions. Other webbing spacing patterns could also be readily accommodated by interchanging a pair of pattern plates if needed. The fixture is designed to support a total load of 100,000 lbs in each direction. For the bi-axial tests described in this paper, a woven panel constructed from 15 hoop webbings (HW) and 9 axial webbings (AW), based on the webbing spacing used on the TransHab test article, was used. It should be noted that it is possible to rotate the panel in the fixture 90 degrees to enable hydraulic loading of the axial webbings if desired (this was not done for this study however). Opposite the actuator end of the test fixture is a stationary load introduction frame that is attached to a backstop.

To introduce load to the webbings in a manner consistent with an actual inflatable article, and to allow for individual load measurements, the load introduction hardware and specimens had to include a number of features. The webbing specimens used a flight-like 8-inch tapered-diamond-stitch lap seam at each end that was also used in the TransHab and has been shown to be about 90% efficient. The lap seam creates a loop that goes over a ¾-inch pin attached to a

clevis, which represents the hardware used at the bulkhead interfaces of the TransHab and subsequent NASA inflatable modules. A threaded rod, attached to the clevis, passes through the 2-inch thick steel pattern plate and a spherical washer that allows the webbing to freely align itself under load. It then passes through a stack-up of two load introduction washers and a 10-kip load washer in the middle, to measure the individual webbing loads at each end. The load washers were customized Pinnacle Sensors FC325-10K load washers, with 10V input, 2mV/V output and a static accuracy of ± 25 lbs. Finally, a nut is used to apply load to the attached webbing. The staggered up/down positions of the load introduction hardware orient the webbings at the correct weave angle at the edge of the woven panel and the clevis design enables the 1-inch wide hoop webbings to lie edge-to-edge as is the case in the actual weave. The 48 load washers (15x2 HW and 9x2 AW), and the actuator load and displacement were recorded on a StrainSmart System 5100 A/B data acquisition (DAQ) system, with the actuator being controlled by an MTS FlexTest SE controller.

Description of Testing

Panel Grid Nomenclature

The bi-axial test woven panel component, consisting of fifteen HWs in the actuator direction and nine AWs in the perpendicular direction, is shown in the Figure 5 schematic. The woven section is 15.5 by 13.625 inches. The HW are spaced 0.02 inch apart while the AW are spaced 0.43 inch apart, interlaced in a plain weave, representing the geometry used on TransHab. There are 135 overlapping sections of the hoop and axial webbings that were identified as interrogation areas for strain measurement via Digital Image Correlation (DIC) photogrammetry. An additional 48 areas, at each end of a webbing outside of the weave, were also interrogated. To identify the overlapping sections a “grid” nomenclature is utilized. Starting at the left, the HW are numbered from one to fifteen from left to right and the AW are numbered from one to nine from bottom to top. The webbing crossings are designated by numbered pairs: (HW,AW). Thus, the center of the weave is referred to as (8,5) indicating hoop webbing 8 and axial webbing 5.

Strain Measurement

The photogrammetry system uses a pair of Point Grey FLEA-2 5MPx digital cameras with Schneider 23mm Xenoplan lenses setup approximately 68 inches above the bi-axial panel and aligned with the grid coordinate system described in the previous section. LED light bars provide an evenly distributed light over the panel. A DIC software package called VIC-3D (Ref. 3) is used to capture and post-process the images from a test to output strains at the identified areas of interest inside (135 locations) and outside (48 locations) of the weave. The DIC software requires a random speckle pattern on the interrogation areas; therefore, the webbings receive a thin coat of white latex paint with black speckles prior to testing. A triangle wave produced by a GW Instek SFG-1003 function generator at 0.1 Hz is captured via an attached National Instruments NI-9215 analog voltage acquisition board along with the strain data in the DIC software. The 0.1 Hz wave is also fed into the StrainSmart DAQ system and used to time-sync all of the sensor data after the test.

Test Sequence

A bi-axial test case begins by first individually preconditioning each of the 24 webbings, to be used in the test panel, in a separate 100-Kip MTS load frame using a second identical photogrammetry setup. Each webbing is put through a 5-cycle loading from 0 to 25% of the tested average ultimate tensile strength (UTS) to represent multiple inflations to the operational pressure of an inflatable structure with the typical safety factor of 4. The strains are computed within the DIC software to produce an area-averaged value for a 10-in. length at the center of the webbing. This repetitive load cycling reduces variability in the load-strain behavior of the webbings. The preconditioning was also performed to address a goal of the testing: to ascertain whether the final-cycle load-strain responses from these individually characterized webbings can be used to convert the DIC strains measured during the biaxial testing to loads in the webbing weave.

Once the preconditioning for each webbing has been completed and recorded, the webbings are then installed in the bi-axial test frame and interwoven to form the test panel shown in Figure 2. The load washers and actuator load cell are then checked and zeroed. The DIC system is calibrated prior to each test (to account for any camera movement that may have occurred between tests), and once that system and the DAQ are set to record data, the test begins. The load is applied to the webbings incrementally in steps by first commanding a set point (SP) load in the hoop webbings via the actuator, then manually adjusting the axial webbing tensions by tightening the nuts one at a time on the self-reacting load frame to a corresponding load level, half that of the hoop webbings. The set points and target loads are provided in Table II. All bi-axial tests incrementally loaded the webbings up to their operational level of 25% of the rated load (3,000 lbs in the hoop and 1,500 lbs in the axial webbings, respectively). Care was taken in order to ensure that the loads were equally distributed among the individual AWs as measured at the boundary load washers. The tension adjustments in the AWs on the self-reacting load frame alternated from side-to-side to keep the panel approximately centered. The set points loads are the desired nominal loads. However, the loads for each webbing were acquired from load washers at each end, and these loads would typically vary somewhat around the nominal as adjustments were made.

Results for four cases conducted over a period of 9 months will be provided, see descriptions in Table III. The primary difference between the cases is the control of the hoop webbings as HW 8 is released. Both ends of hoop webbing 8 were simultaneously released to simulate the loss of a webbing. The webbing was released by manually loosening the nuts shown in Figure 4 over a period less than 10 seconds. In Cases A and B, once the maximum load at Set Point 4 (SP4) was reached then the actuator displacement was fixed, hence the designation “displacement-controlled”. In these cases, the total load decreases about 3,000 lbs as HW 8 is released. For cases C and D, once SP4 is reached, the actuator load is commanded to retain the total load as HW 8 is released, hence the designation “load-controlled”. The load-control cases more closely resemble loading for a deployed habitat as the internal pressure is nominally constant.

Strain Post-Processing

The photogrammetry system is capable of extracting strains in multiple ways from the areas of interest. Figure 6 details a comparison of several of these approaches; the image at the

top is of a representative HW under load with longitudinal strain contours superimposed. Strain can be measured as the average of a selected area, or a virtual extensometer can be placed to get a point reading at any desired location. Areas for averaging strains are denoted by the red rectangle “R6” and the white squares “R2” and “R3”. In addition, three virtual extensometers span each area R2 (E6, E7, E8) and R3 (E9, E10, E11). Load-strain results for each of the methods are provided in the bottom graphs. The virtual extensometer strains are computed based on the relative change in distance between two points, while the area-averaged strains are computed within the DIC system over an area specified by the user. Nearly the entire field of view is encompassed by the red rectangle designated as R6, while the localized area strains, R2 and R3, more closely replicate the area that will be extracted in the woven section during the bi-axial load testing. Visual inspection of the top figure shows a large variation in strain along the length of the webbing. To a lesser extent, there is also variation across the webbing width. These results indicate: there exists a large variation in the initial strain behavior at varying longitudinal locations; at the R2 location the webbing loads up much faster than at R3, (i.e. less initial dead band); and R6 data falls between the curves for R2 and R3. It was decided that extraction of a large amount of virtual extensometer data would provide little if any benefit to improve understanding of the effect of a webbing failure. Subsequently, strains will be extracted using area-averaged values for the bi-axial load testing. It should be noted that this particular webbing had been tested previously in the bi-axial test fixture, and the lower and higher strain zones shown corresponded to where the axial webbings crossed this strap. A pristine strap does not show this type of variation prior to weaving. This data did illustrate however that care must be taken in the post-processing and load-strain analysis and demonstrated the impact of weaving the webbings on the load-strain behavior, especially given that the strap used in the biaxial test didn’t have observable surface differences to the pristine strap that would suggest the observed strain behavior a priori.

Area-averaged load-strain measurements for areas R0 through R6 are provided in Figure 7. As before, R6 spans the field of view, while R0-R5 are selected squares within R6. The raw data are provided in the lower-left plot. Based on visual inspection, it appears that after the initial loading, all of the curves follow a similar profile. It was decided to adjust the strains on each curve by subtracting the corresponding strain at a low load level. For this example, the level closest to the HW load at SP1 (200 lbs) was 211 lbs as measured on a load washer. The results after the strain adjustments show that the curves nearly overlay, Figure 7(b). A primary purpose of the testing is to understand the load behavior by taking measured strains and converting them to loads via the webbing load-strain curves. Thus, the strain itself is not of primary interest. For this reason, it was decided to adjust each measured strain history by re-zeroing it at a low load. This is often done in extracting load-strain or load-displacement data for softgoods given the variance in the initial, almost zero-load extension behavior that is due to decrimping of the interwoven yarns in the webbings. For the bi-axial load testing, the strains at SP1 were selected as the reference point for re-zeroing.

Test Results and Discussion

Referring to Figure 5 and starting at the center of the section, Zone “A” is the area within the weave that is removed from the boundary by 2 webbings. Zone “B” is the area within the weave, but outside Zone A. Zone B results are not of interest for this paper as they are a transition

zone. Zone "C" measurements are located outside of the weave. The measurements in Zone C are particularly useful for assessing the strain-to-load measurement approach as the load in each webbing is known from the load washer data. Finally, the dashed purple lines highlight the central webbings that will be the focus in many of the figures.

A comprehensive set of data figures will be provided for Case C, conducted in July 2019. This case was selected since the test was conducted using load control throughout for the hoop webbings. The detailed time history results are provided in Figures 8 through 13. (The corresponding history results for the three remaining test cases are provided in Appendix A). The time history plots will generally follow the same pattern for each figure. Specifically, subplot (a) in the upper left contains all of the associated histories, while subplots (b)-(d) will contain a subset of histories related to either the hoop webbings (7, 8, and 9) or the axial webbings (4, 5, and 6). Anomalous data are identified on the graphs. Following the detailed history results for Case C, selected summary results incorporating all four cases will be provided.

Time histories for Case C

The time histories from the load washers for the HWs are shown in Figure 8. As noted in subplot (a), the load for HW 5 (Bottom) read consistently lower than the remaining webbings. It is likely this was either an issue with the load washer itself or from a mounting irregularity. It should be noted that the loads measured for HW 5 (Top) did not read low. Since the total load top vs bottom is similar, it is not likely related to a calibration or transducer issue. Although the actuator is commanded to apply a total load of 45,000 lbs at SP4 (i.e. 3,000 lbs average load per HW), the summation of the load read by the load washers for the HWs is 43,649 lbs for the top and 43,500 lbs for the bottom locations, see Table IV. The nearly 1,500 lbs difference between the commanded and summation of measured loads is evident in the mean of the webbing loads, namely, 2,910 lbs for the top and 2,900 lbs for the bottom locations. The corresponding standard deviation for the top load washers is 150 lbs, while that of the bottom load washers is 230 lbs. Therefore, the resulting normalized standard deviation (σ/μ) is 0.0515 for the top and 0.0793 for the bottom locations. Given that all of the hoop webbings are attached to one actuator, it is interesting to note that there is a significant variation in load prior to HW 8 release. Ideally, the HW load washers would read 3,000 lbs each at SP4. Looking more closely at the focus webbings (subplots (b)-(d)), these results show that the load washers on the bottom are measuring slightly higher than those on the top. As expected, the loads in HW 8 drop to nearly zero at 126 min, when HW 8 is released, see subplot (c). After webbing 8 is released, the loads in the two neighboring webbings, i.e., HW 7 and 9, increase 100 lbs at the top and 120 lbs at the bottom. Based on a summation of the load washers, the total load carried by the webbings decreases ~ 70 lbs, such that after release the loads are 43,579 lbs and 43,427 lbs for the top and bottom locations, respectively.

The corresponding axial webbing loads are provided in Figure 9. There is an obvious relaxation of the loads from 50 min to 80 min, at which time the AW are manually re-adjusted one-at-a-time prior to the release of HW 8 at 126 min. There is a small but distinct difference between the loads measured by the load washers attached at the left side of the weave and those measured on the right side. The mean loads for the AW at SP4 are 1,516 and 1,430 lbs, for the left and right ends of the webbings, respectively, see Table V. The corresponding standard deviations are 12 and 18 lbs, which result in a normalized standard deviation of 0.0079 and

0.0126 for left and right locations, respectively. At the time that HW 8 is released at 126 min, the AW 4 and 6 load washers, subplots (b) and (d), respectively, show a slight decrease in load, while there is no significant change in the load in AW 5, subplot (c).

Measured strains in Zone C are provided in Figures 10 and 11 for the HWs and AWs, respectively. As a reminder, these are the average strains, located just outside the weave, computed by the photogrammetry software over an area approximately 0.9 x 0.9 inches. The anomalous results for the HW are all located at the "Top", see Figure 4. As the webbing load washers did not reflect this anomalous behavior, the behavior is most likely related to the data extraction and post-processing, due to an anomalous change in the pattern or lighting of the pattern that the photogrammetry system is tracking. These results highlight the benefit of extracting and reviewing data from multiple sources and locations. Following HW 8 release, the strains in HW 8 do not return to zero. This could be anticipated following review of the preconditioning unloading curve, where the strains do not return to zero at zero load. Comparing load washer and strain data, the corresponding load washer data for HW 8, see Figure 8(c), does not show a significant difference between the top and bottom loads. Unlike the hoop webbings, the variation is very small for the Zone-C AW strains. It should be noted that the relaxation behavior for the loads between 50 min and 80 min, Figure 8, are not evident in the corresponding strains.

Finally, the strain histories from Zone A are provided for the HWs and the AWs in Figure 12 and 13, respectively. First focusing on the HW histories provided in Figure 12. As for Zone C, small changes are seen at 80 min, when the axial webbings are re-adjusted. The strains in HW 7 and 9, subplots (b) and (d), respectively decrease when HW 8 is released at 126 min. On the other hand, with the exception of a temporary increase, the strains in HW 8 (subplot (c)) change very little after the HW is released. These trends in strains do not align with the trends for the load washers and the strains in Zone C. The AW Zone-A strains are provided in see Figure 13. The relatively wide variation was not anticipated, based on the small variation for the Zone-C axial webbing strains shown in Figure 11. One possible explanation for these results: as HW 8 is released, the axial webbings crossing it hold it in place due to friction at the cross-over points, absorbing some of the load in shear. As this occurs, HW 7 and 9 actually get a slight reduction in load in the weave due to the axial webbings moving in the direction of HW 8 and pulling in slightly on HW 7 and 9. Additional testing may be required to fully understand the physical phenomena.

Summary results for four cases

At this point, summary results incorporating data from all four cases will be provided. The summary results enable comparison of similarities and differences in trends across the four test cases. For consistency from figure-to-figure, color designations have been chosen such that Case A is shown in green, Case B in blue, Case C in black, and Case D in magenta.

Load washer results at SP4 are provided in Figure 14, with the corresponding statistics provided in Table IV. In each graph, the x-axis corresponds to the webbing number shown in Figure 5. There is more webbing-to-webbing variation for HWs (subplots (a) and (b)) than for the AWs (subplots (c) and (d)). It is interesting to note that there are global magnitude differences between the cases. Little variation in AW loads would be anticipated, since the webbings are manually tightened. The load washer for the bottom location of HW 5 is consistently lower for all the cases as has been noted previously. The corresponding Zone C strains are shown in Figure 15.

As for the AW load washers, the corresponding Zone C strains show little variation. The small global differences seen in the loads seem to be amplified in the strains. Large variations in strains in the HW 1 through 5 Top locations are evident. These large variations are not evident in corresponding Bottom locations for HW 1 through 5. It should be noted that the low load for HW 5, Figure 14 (b), is not reflected in the associated strains.

At this point, the evaluations will transition from behavior at SP4 to understanding the impact of HW 8 release on loads and strains. Strain histories for HW 7, 8, and 9 are shown in Figure 16 for all cases. The time of HW 8 release varies from case to case and has been noted in the table. The trends previously observed for Case C are replicated in the remaining test cases. Namely, the strains in HW 7 and 9 decrease, see subplots (a) and (c), while those in HW 8 show little change, see subplot (b). This consistency in trends is particularly noteworthy since the tests were conducted over a 9-month timespan and the webbings were changed and rewoven multiple times. Additional plots focusing on Zone A strains are provided in Figure 17 for AW crossing HW 8 and in Figure 18 for HW crossing AW 5. As before, the data for each test case are provided on separate graphs, with the legends identifying the particular location for the measurement. Each of the AW locations shows an increase as it crosses HW 8, when HW 8 is released. This change in behavior again seems to indicate that the load is transferred from hoop to axial webbings. A different way to look at load transfer is through the strains as the hoop webbings cross AW 5, see Figure 18. In this case, the strains in HW 7 and 9 decrease where they cross AW 5, but other webbings see a small increase or no change. This unexpected load transfer in Zone A has been identified as an area for future study. Hammer testing beyond that shown in Appendix C could provide insight to support or not support the Zone A strain behavior, as it may be possible to determine changes in stiffness in the webbings via changes in the measured wave propagations.

The change in measured load resulting from release of HW 8 on both the hoop and axial webbings are provided in Figure 19 and Table VI. The data is computed by taking the load at SP5 (or immediately after release) and subtracting the load at SP4. A few general observations: the loads in HW 1-6 and 10-15 increase ~ 200 lbs for the load-controlled cases and ~ 50 lbs for the displacement-controlled cases; while HW 7 and 9 increase approximately 100 lbs for the load-controlled cases and are actually less than zero for the displacement-controlled cases. Also note the distinct “sawtooth” pattern when traversing across the webbings. The even webbings increase more than the odd webbings. This is likely due to a rotation or flexure of the fixture. A modest sawtooth pattern was also observed for the HW loads, in Figure 14, indicating that even prior to HW 8 release, there was an imbalance between the odd and even webbings. The corresponding results for the left and right load washers attached to the AWs are provided in subplots (c) and (d), respectively. The sawtooth pattern is also evident here. The release of HW 8 caused the axial webbing loads to decrease approximately 10 lbs.

Finally, for each webbing, the strains measured during the pre-conditioning tests were extracted using an area similar in size to R6 in Figure 6. Sample load-strain curves using pre-conditioned data from Case C are shown in Figure 20 for the final or 5^{th} cycle. The corresponding statistics are provided in Table VII. For the hoop webbings, the loads are extracted at strains of 0.004 and 0.008 in/in. For the axial webbings, the loads are extracted at 0.006 and 0.012 in/in. These curves and their associated statistics are intended to provide: a measure of the uncertainty of the measured load given a measured strain; and a quantification of the uncertainty to use in

probabilistic models. No pre-conditioning data is available for Case D due to an issue with the test setup.

As mentioned previously, one desired use for the pre-conditioning load-strain curves was to be able to convert the measured area-averaged strains into webbing loads. As a check on this approach, in-situ load-strain curves were generated from the load washer data and Zone C strain measurements acquired from SP1 through SP4. For example, for HW 7, the load washer data from the top was plotted against the Zone C top strains, output from the DIC system. Thus, for each test case 30 hoop load-strain curves were generated along with 18 axial load-strain curves. The hoop webbing curves were averaged as were the axial webbing curves. The comparisons of the average pre-conditioned and in-situ Zone C load-strain curves are provided in Figures 21 and 22 for the hoop and axial webbings, respectively. Subplot (a) in each figure provides a comparison of the average pre-conditioning curves for Cases A, B and C. No results will be provided for Case D. Focusing first on the hoop results in Figure 21, the pre-conditioning curves for the 3 cases nearly overlay. However, a review of subplots (b)-(d) would indicate a softer in-situ webbing behavior than was observed during the pre-conditioning uni-axial test phase. The axial webbing shown in Figure 22 displays a similar trend. It had been expected that the in-situ Zone C load-strain curves would overlay on the pre-conditioning curves. These results would suggest that the pre-conditioning load-strain curves are not appropriate to use to infer the webbing loads based on measured strains. Potential sources of the discrepancy observed between the pre-conditioned and in-situ Zone C webbing load-strain curves need to be investigated further.

Concluding Remarks

A series of bi-axial load tests of a representative woven-panel component of a softgoods habitat were conducted. The data from this representative softgoods component were acquired: 1) to aid in understanding the load transfer within the weave once a webbing fails; 2) to evaluate strains derived from photogrammetry as a means for monitoring loads and structural integrity; and 3) to support numerical model development. The planar test-section was composed of 15 HW and 9 AW, with the webbings attached to a frame well-outside the test-section. Loading of the HW was done by fixing one end of the webbings, while a pneumatic actuator imparted a load to a movable frame holding the opposite ends. The AW loads were manually adjusted one-at-a-time to a specified load prior to each set point. In addition to the load washers at the end of each webbing, strains were measured on the surface of the webbings using a photogrammetry system relying on a digital image correlation (DIC) technique.

Results were evaluated as time histories, as well as summary data extracted at specific load set points. The following observations were made:

1) Strain data should be averaged over an area, with the data reported relative to the strain at a low load level, in this case SP1, to remove the strain variability due to initial tensioning in each webbing.
2) The results for the four test cases, conducted over a span of 9 months, showed similar trends with regard to webbing loads and strains. However, absolute strain magnitudes did vary from case to case.
3) A rotation or flexure of the webbing restraint fixture was observed by monitoring the change in load due to the release of HW 8. This rotation or flexure was identified by the distinctive

sawtooth pattern resulting from whether the webbing was attached to an upper or lower pin on the frame. This is true for both the hoop and the axial webbings.

4) The webbing behavior **outside the weave** when HW 8 is released was as **expected**:
   - The loads for the load-control cases in the HW increased ~200 lbs, although the loads in the immediate neighboring webbings increased ~ 100 lbs
   - The loads in the AW Zone C decrease slightly, or ~ 10 lbs
   - The measured strains for both the HW and AW generally follow the load trends
5) The trends **within the weave** when HW 8 is released were **unexpected**:
   - The strains for the released HW 8 change little
   - On the other hand, the strains in the neighboring hoop webbings decrease significantly
   - The strains in the axial webbings increased as they cross the released hoop webbing.
6) **It appears that for a woven-webbing restraint layer, the strains extracted using the photogrammetry method cannot be used to accurately calculate the webbing loads.**
7) Nonetheless, the commonality of the trends across the four cases, whether displacement-controlled or load-controlled, provides some confidence that the trends could be replicated in a numerical model simulation. For this reason, further development of the finite element model is planned to support understanding of the physics and the parameters that contribute to the observed behavior.

The following are suggestions for follow-on testing work.

1) Explore the implementation of an alternative approach to measuring loads/strains within the weave.
2) Ascertain whether the test set-up significantly impacts trends within the weave, examples include:
   - Instead of releasing hoop webbing 8, release hoop webbing 9 or axial webbing 5.
   - Release a webbing from only one end, rather than both concurrently.
   - Increase number of axial webbings
   - Design test for a webbing failure within the weave
3) The primary focus of the data provided in this document was to help understand the detailed or local behavior of the webbings, particularly when one webbing was released. A complementary use of the data was to begin understanding of the global behavior of the entire woven component, as provided in Appendix B.
4) The exploratory hammer testing results provided in Appendix C, show promise for providing additional data to support understanding of how the structural responses are affected by the release of a webbing.
5) Investigate potential sources of the discrepancy observed between the pre-conditioned and the in-situ Zone C webbing load-strain curves.
6) A limitation of the test fixture is that the webbings are loaded in a plane and thus do not accurately reproduce the curvature induced in the inflatable vessel as it is pressurized. An inflatable bladder bag that could approximate the deployed curvature of an inflatable vessel and provide the appropriate webbing-to-webbing contact interaction within the weave could be added. This enhancement however would add an additional level of complexity to both the testing and modeling efforts.

Acknowledgements

The authors would like to recognize the contributions of Mr. Alberto Makino (NASA Ames Research Center), who provided the preliminary model.

References

[1] Fuente, H., Raboin, J. L., Spexarth, G. R., and Valle, G. D., "Transhab: NASA's Large-Scale Inflatable Spacecraft", *AIAA Structural Dynamics and Materials Conference*, AIAA-2000-1822, Atlanta, GA, 2000.

[2] Daniel R. Mulville. Structural design and test factors of safety for spaceflight hardware. Technical Standard NASA-STD-5001B w/Ch 2, NASA, October 5, 2016.

[3] VIC-3D Software Manual. Correlated Solutions. Version 8.

Table I. Material specifications for test webbings.

	Designation	
	Vectran 6,000 lb Rated Webbing (AW)	**Vectran 12,500 lb Rating Webbing (HW)**
Type	6996-1 Natural "R" Vectran Webbing	1" Natural Vectran Webbing (100% Vectran)
Specification	Mil-T-87130 Type VI Class 9 Mod to R	Mil-T-87130 Type VI Class 11 Mod to R
Put-up	25 Yd Rolls (-0/+1)	50 Yd Rolls
Vendor	Bally Ribbon	Offray Specialty Narrow Fabrics

** Finish on all webbing: Mil-W-27265E "R" – Polyvinyl Butyral Resin **

Table II. Loading set points.

	Target Webbing Load, lb	
Set Point (SP)	**Hoop**	**Axial**
1	200	100
2	600	300
3	1000	500
4	3000	1500
5 (post-failure)	3000	1500

Table III. Test case designation.

Case	**Month (Year)**	**Actuator Control**
A	Dec (2018)	Displacement
B	May (2019)	Displacement
C	Jul (2019)	Load
D	Aug (2019)	Load

Table IV. HW load statistics summary.

Case	Location	Load (SP4 – Before Release), lbs			Load (SP5 – After Release), lbs
		Mean	Std	Total	Total
A	Top	2897	126	43,457	41,129
	Bottom	2898	229	43,462	41,059
B	Top	2909	164	43,630	40,484
	Bottom	2891	207	43,364	40,155
C	Top	2910	150	43,649	43,579
	Bottom	2900	230	43,500	43,427
D	Top	2905	101	43,570	43,489
	Bottom	2902	202	43,522	43,484

Table V. AW load statistics summary

Case	Location	Load (SP4 – Before Release), lbs			Load (SP5 – After Release), lbs
		Mean	Std	Total	Total
A	Left	1446	20	13,018	12,881
	Right	1411	30	12,701	12,594
B	Left	1519	11	13,673	13,566
	Right	1466	14	13,193	13,099
C	Left	1516	12	13,639	13,551
	Right	1430	18	12,867	12,783
D	Left	1516	7	13,642	13,601
	Right	1503	10	13,528	13,498

Table VI. Statistics for load change resulting from HW 8 release.

Case	Mean change in load, lbs			
	HW [1-6, 10-15]		AW [1-9]	
	Top	Bottom	Left	Right
A	43	44	-15	-12
B	44	44	-12	-10
C	208	210	-10	-9
D	219	220	-5	-3

** HW 7-9 omitted from statistics.

Table VII. Statistics of pre-conditioned strap load-strain curves

Hoop webbing								
	at ε = 0.004 in/in				at ε = 0.008 in/in			
Case	Min	Max	Mean	Std Dev	Min	Max	Mean	Std Dev
A	1448	1600	1544	40	3150	3734	3445	130
B	1304	1620	1479	79	3176	3401	3275	74
C	1386	1498	1455	35	3221	23408	3305	58
D	N/A				N/A			
Axial webbing								
	at ε = 0.006 in/in				at ε = 0.012 in/in			
A	833	954	895	33	1796	1993	1922	58
B	731	814	780	33	1523	1663	1593	59
C	883	945	917	17	1868	1978	1943	41
D	N/A				N/A			

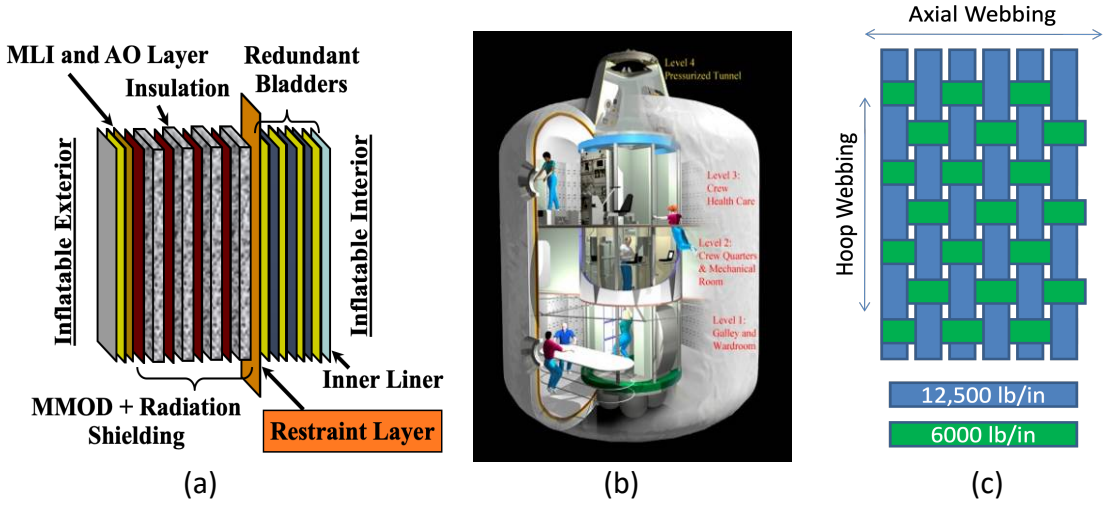

Figure 1. Schematics of the a) multi-layer inflatable structure, b) TransHab, and c) restraint layer weave.

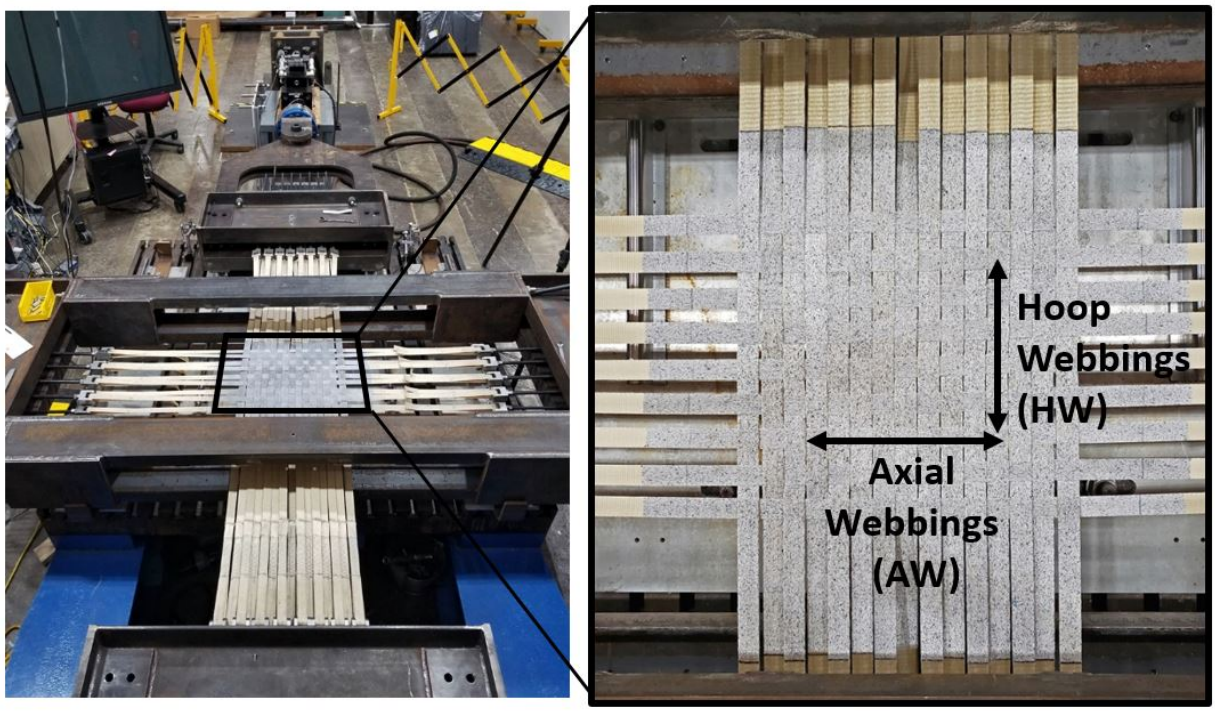

Figure 2. Photographs from test setup

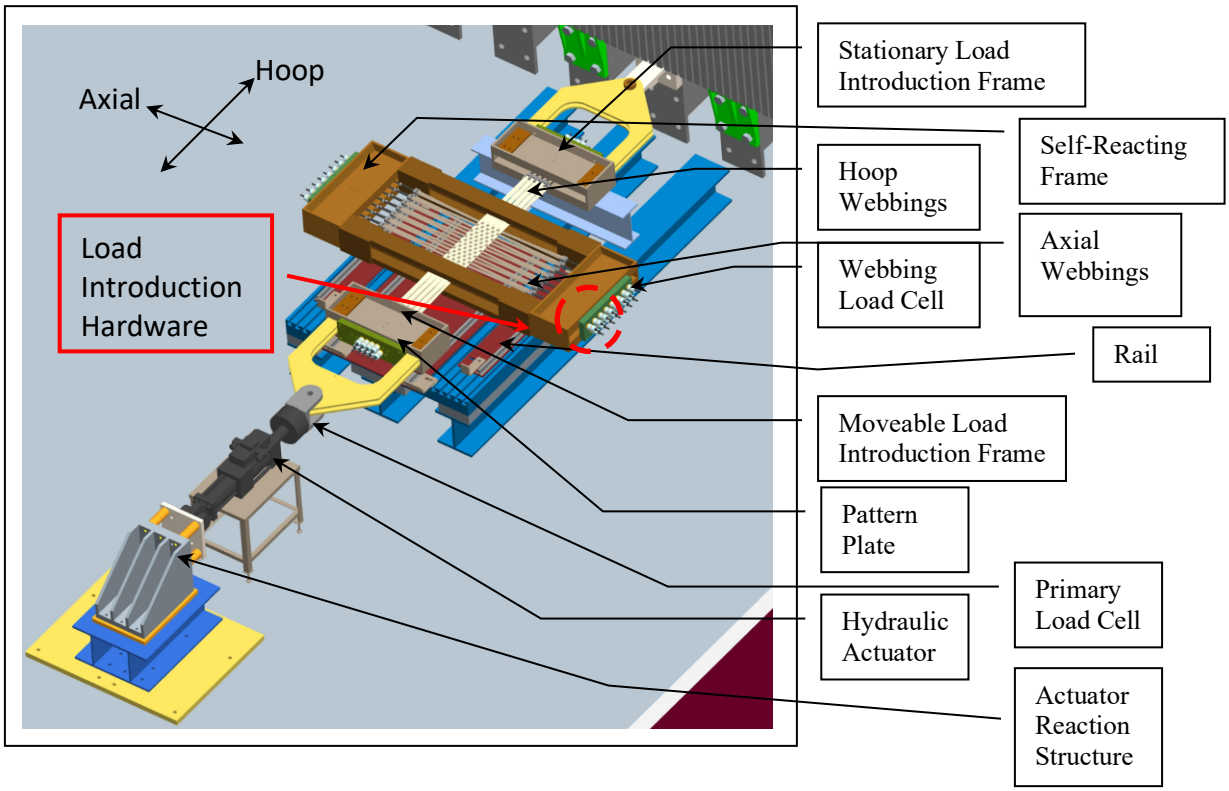

Figure 3. Schematic of test fixture with nomenclature and a notional webbing configuration.

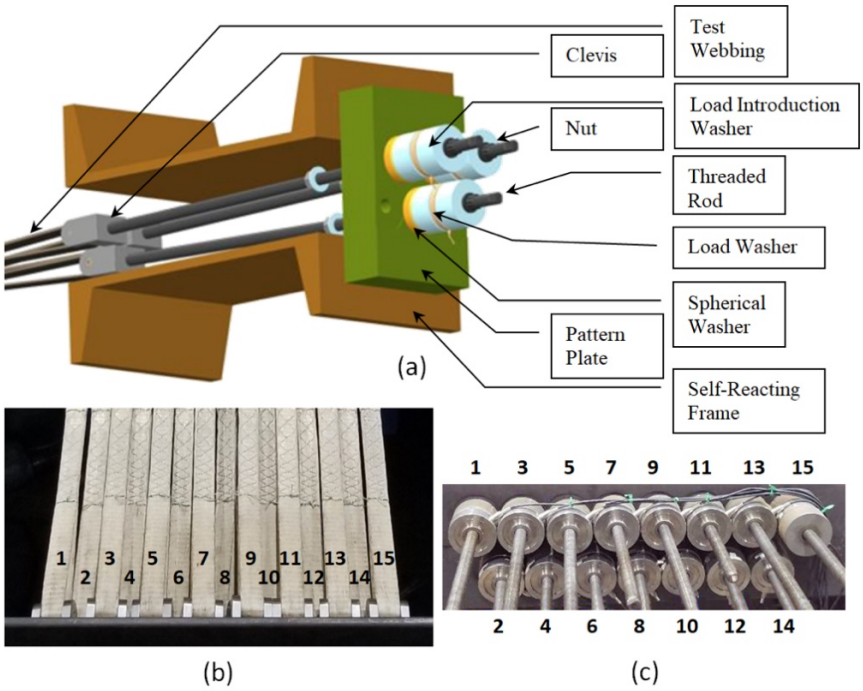

Figure 4. Detail of the hoop webbing load introduction hardware: a) schematic of hardware; b) top view of HW at frame; and c) end view of load washer placement.

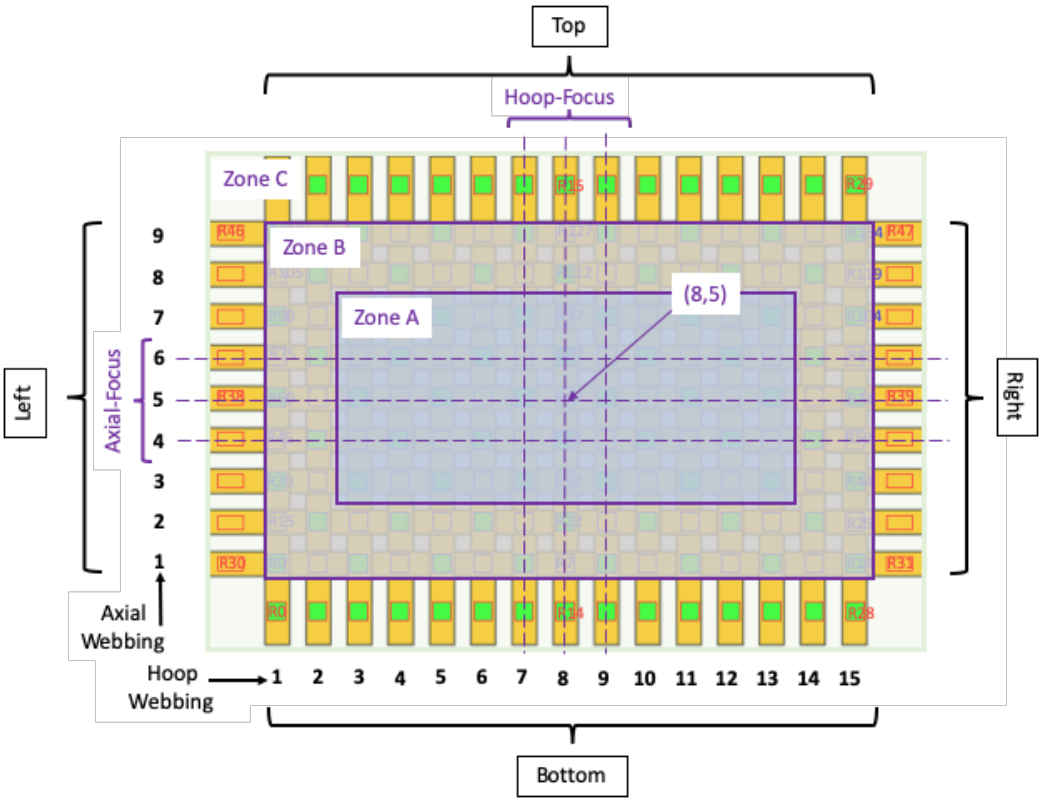

Figure 5. Schematic of test section with zone designations (not to scale).

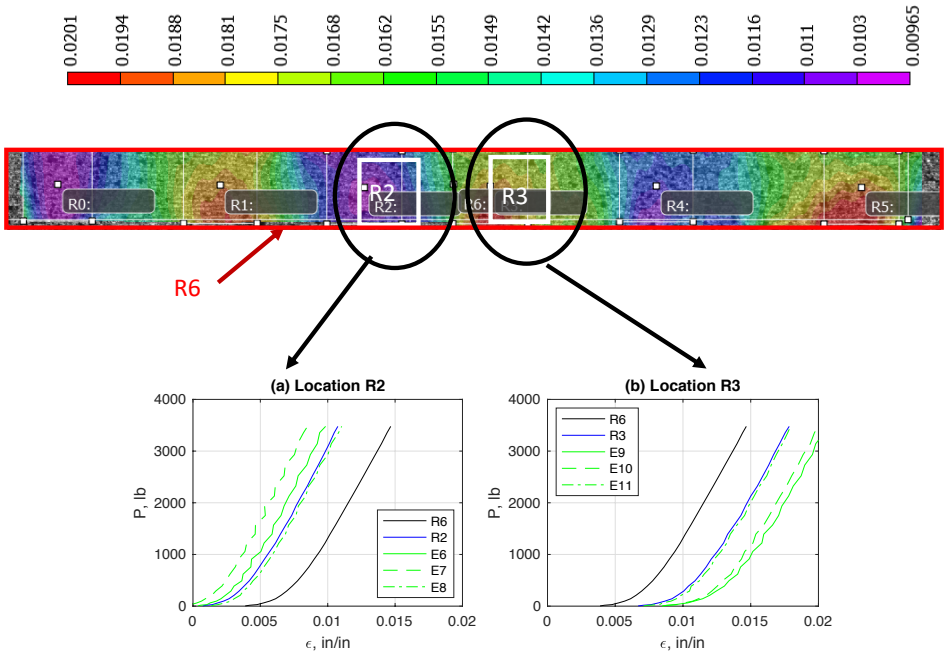

Figure 6. Comparison of different methods for extracting strains (R=area strain, E=virtual extensometer strain).

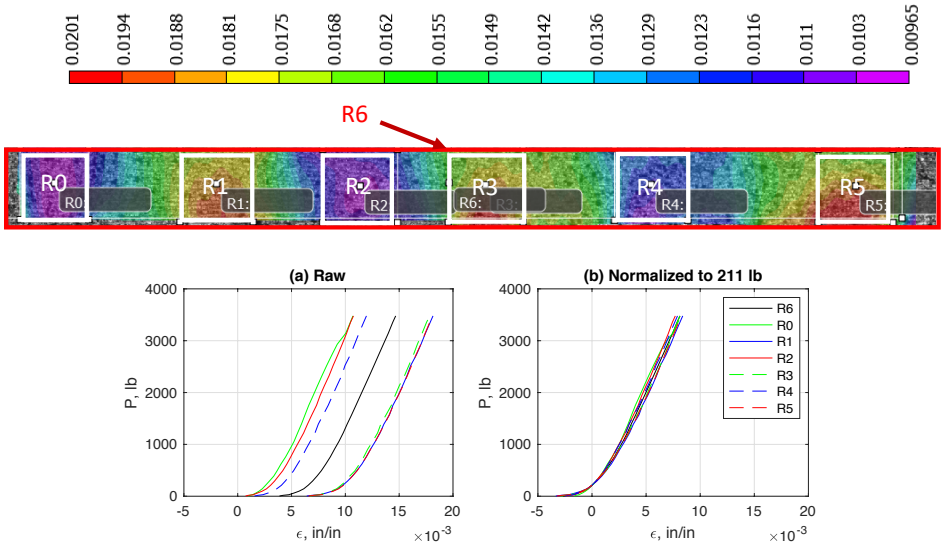

Figure 7. Impact of normalizing strains to a low load.

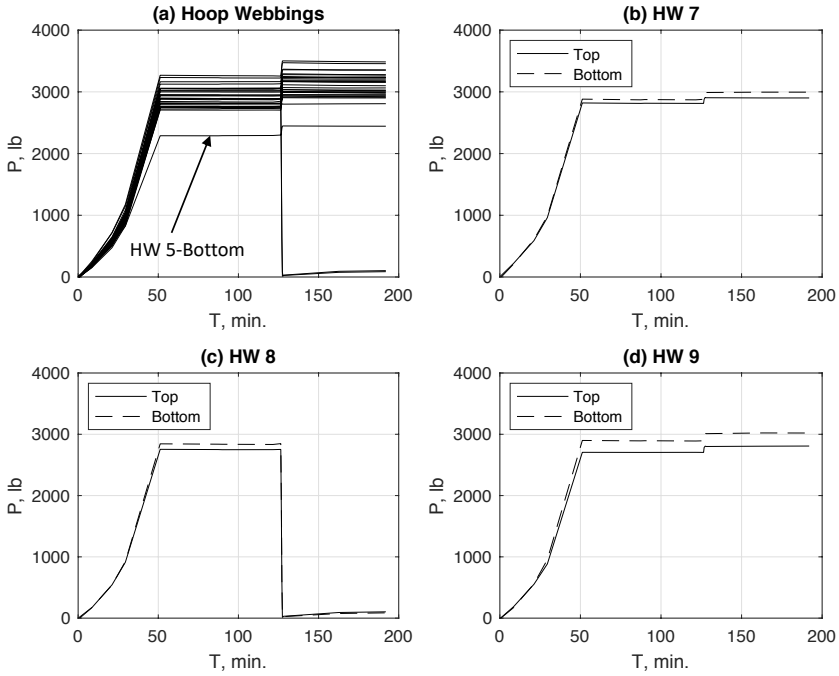

Figure 8. Load histories for hoop webbings [Case C].

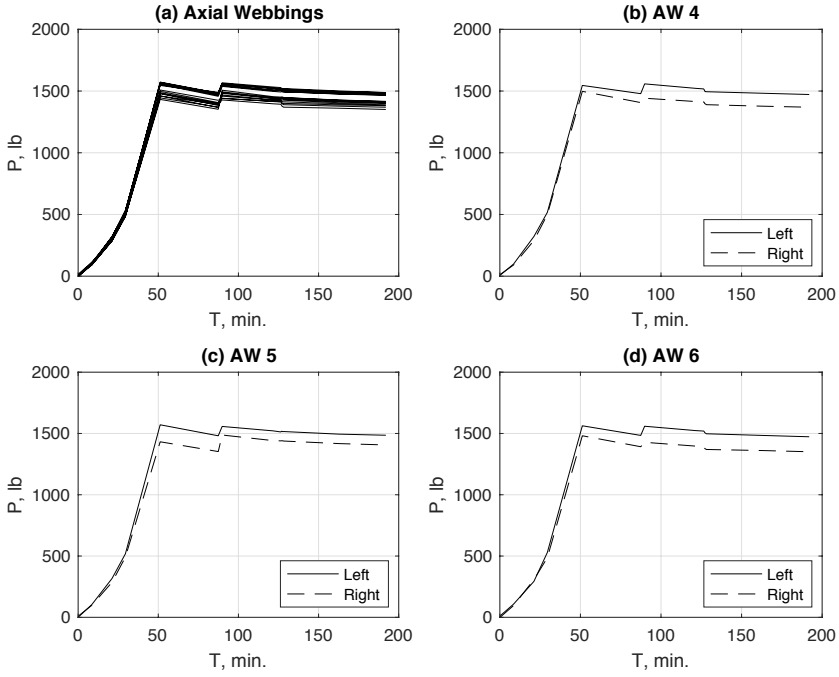

Figure 9. Load histories for axial webbings [Case C].

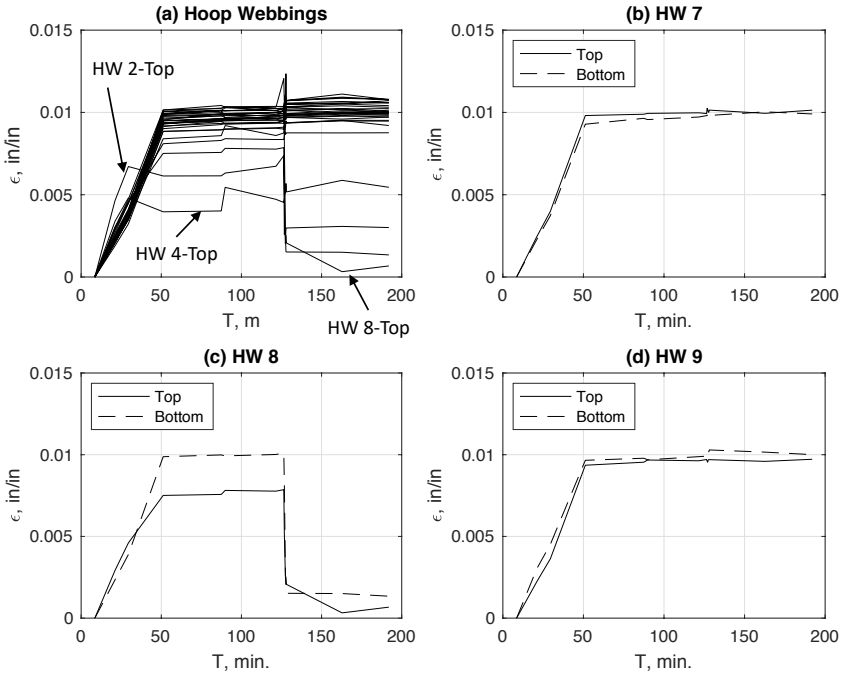

Figure 10. Zone-C strain histories for hoop webbings [Case C].

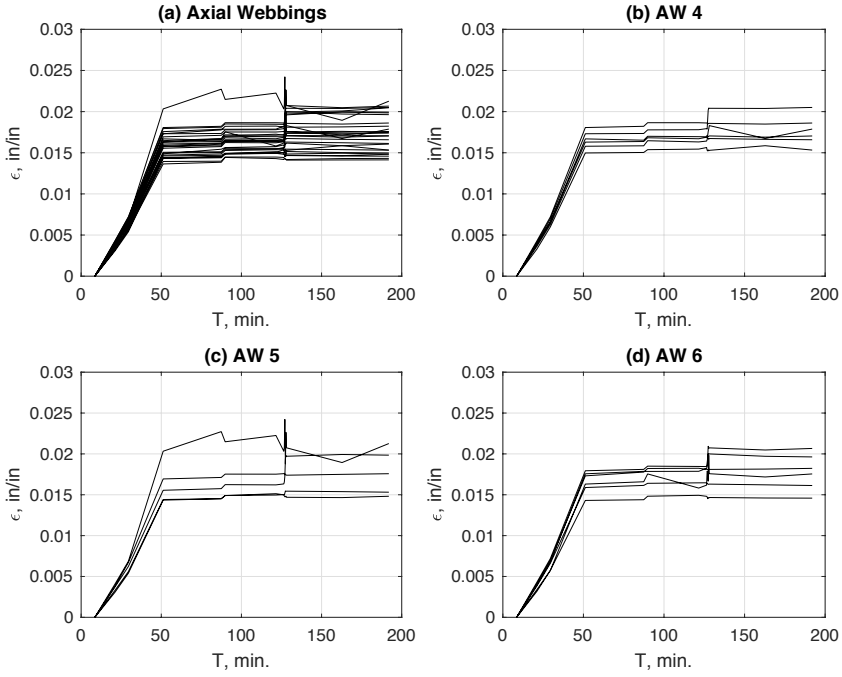

Figure 11. Zone-C strain histories for axial webbings [Case C].

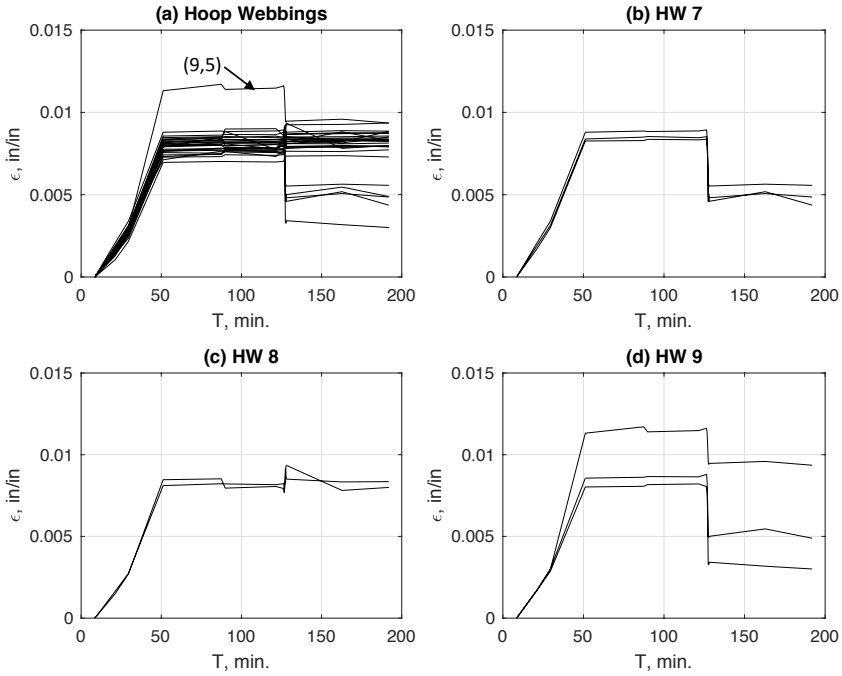

Figure 12. Zone-A strain histories for hoop webbings [Case C].

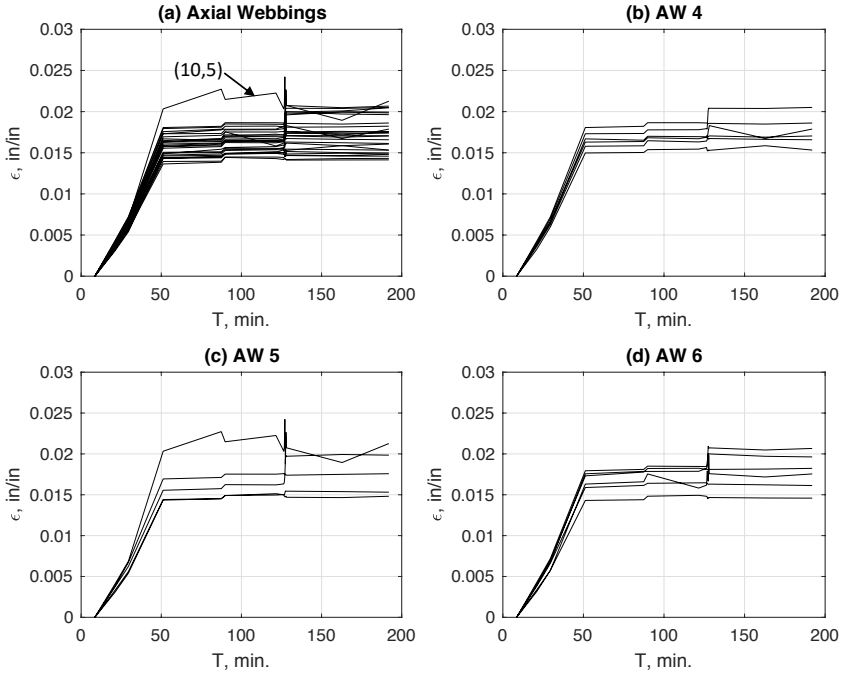

Figure 13. Zone-A strain histories for axial webbings [Case C].

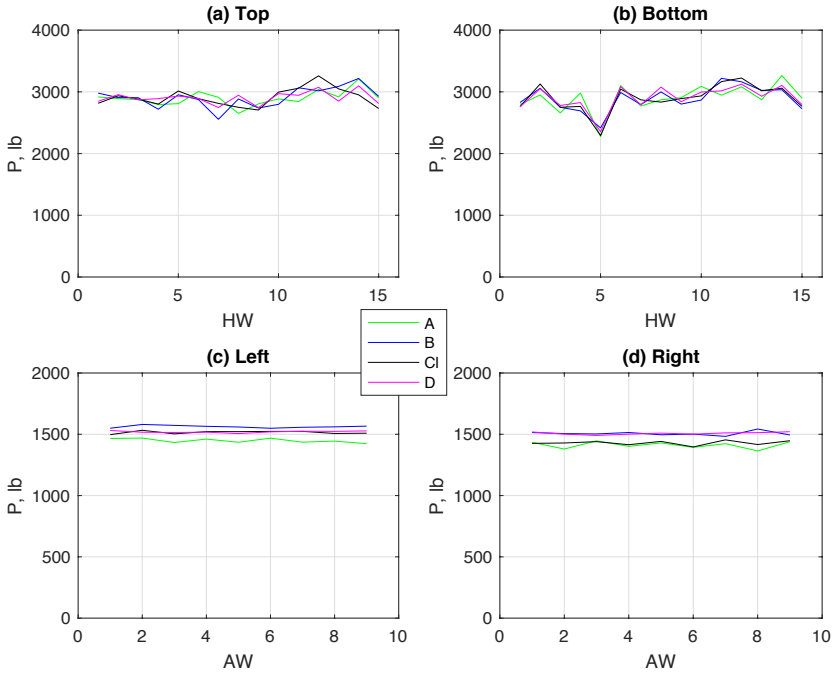

Figure 14. Webbing loads at SP 4.

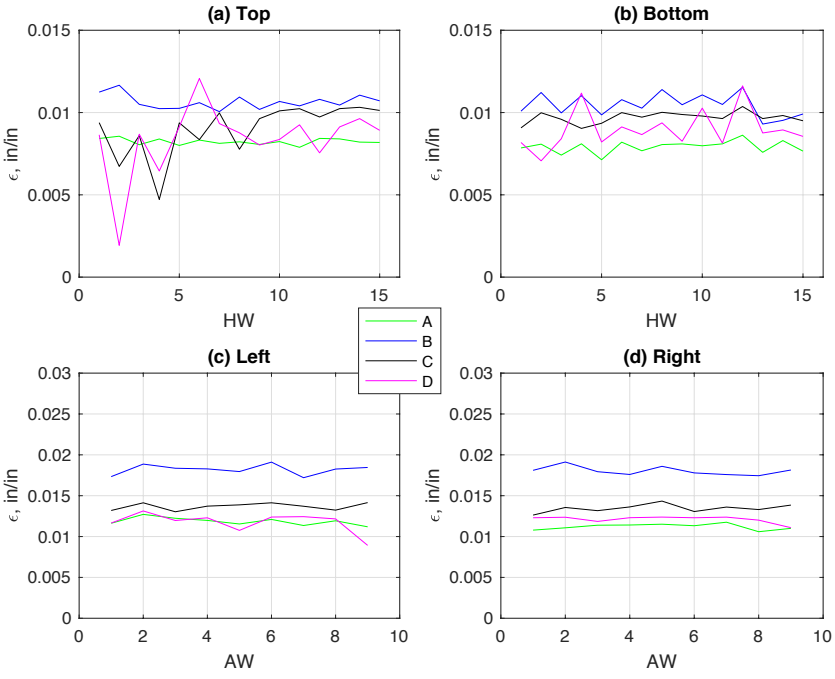

Figure 15. Zone-C strains at SP 4.

Case	Strap 8 release time, min
A	86
B	142
C	126
D	136

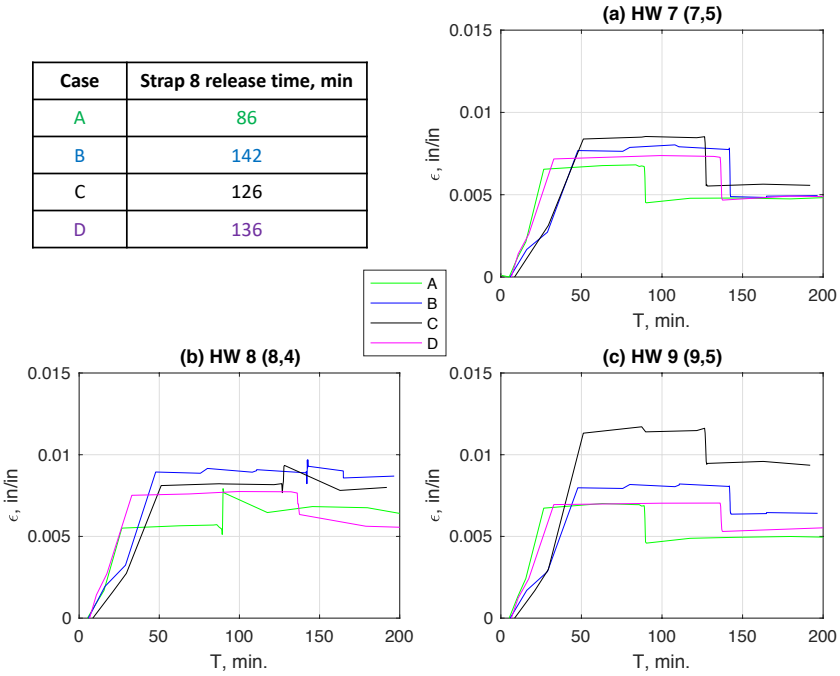

Figure 16. Sample Zone-A strain histories.

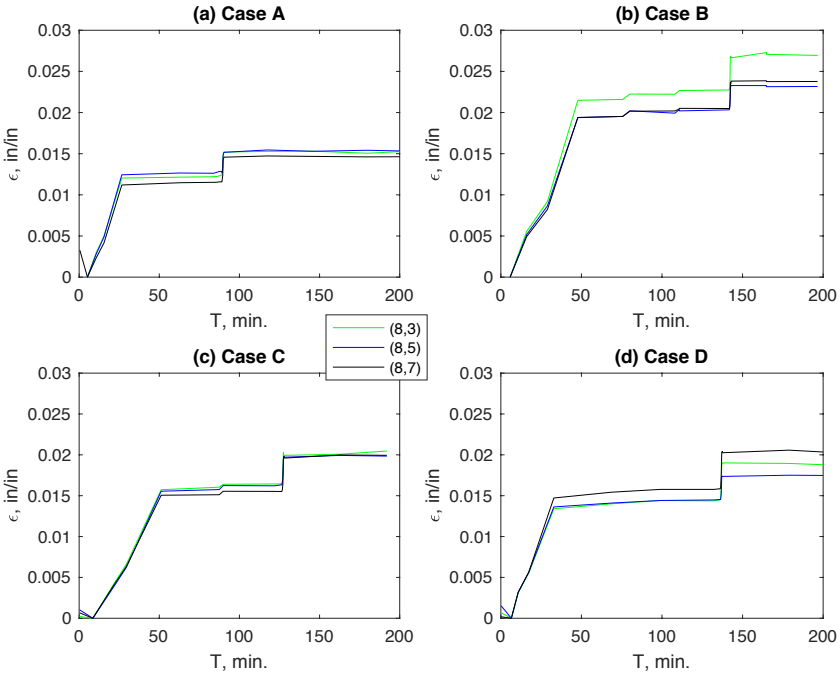

Figure 17. Zone-A axial webbings crossing HW 8.

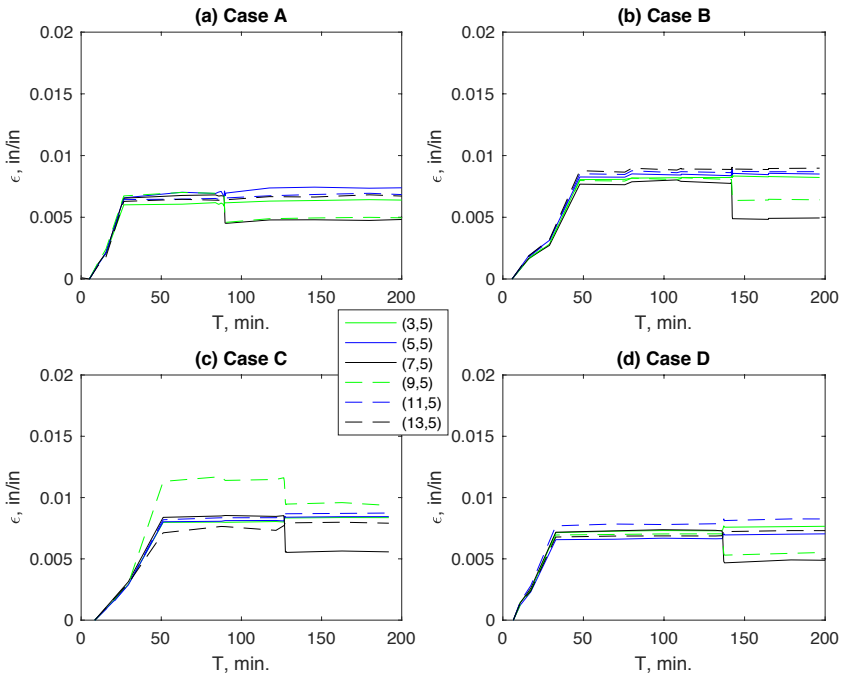

Figure 18. Zone-A hoop webbings crossing AW 5.

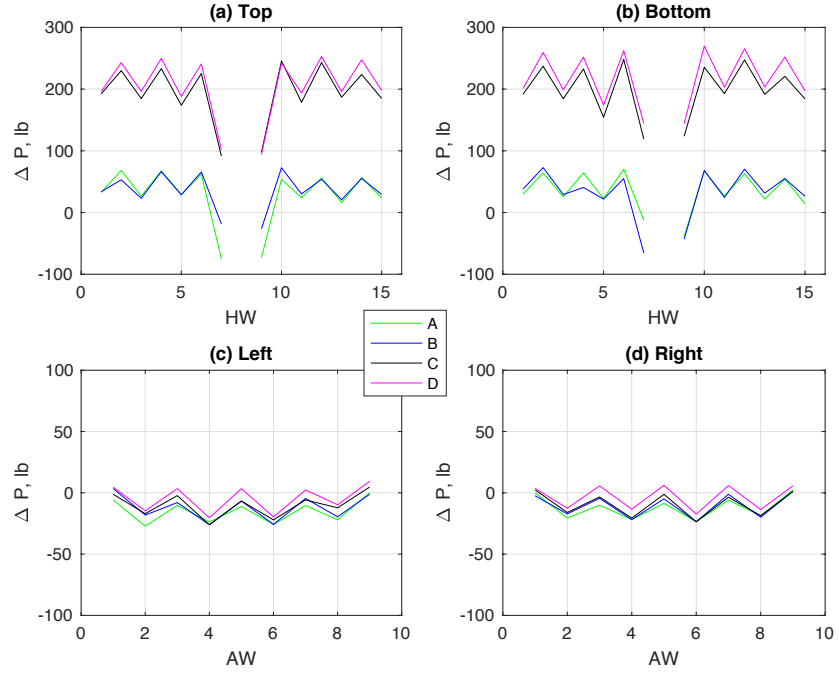

Figure 19. Effect of HW 8 release on strap loads [Note HW 8 has been omitted as the change in load is approximately -3000 lbs].

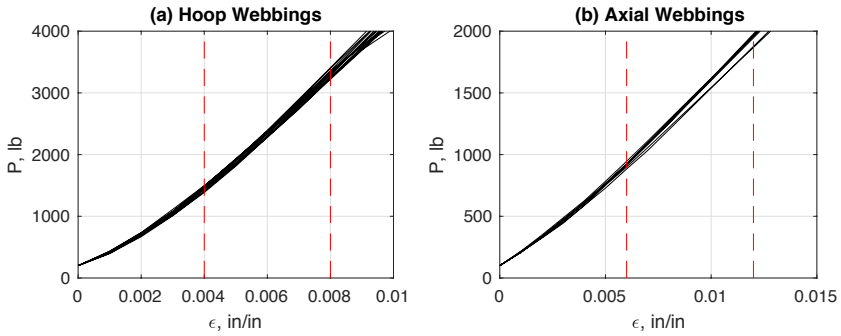

Figure 20. Samples of load-strain curves to compute load statistics.

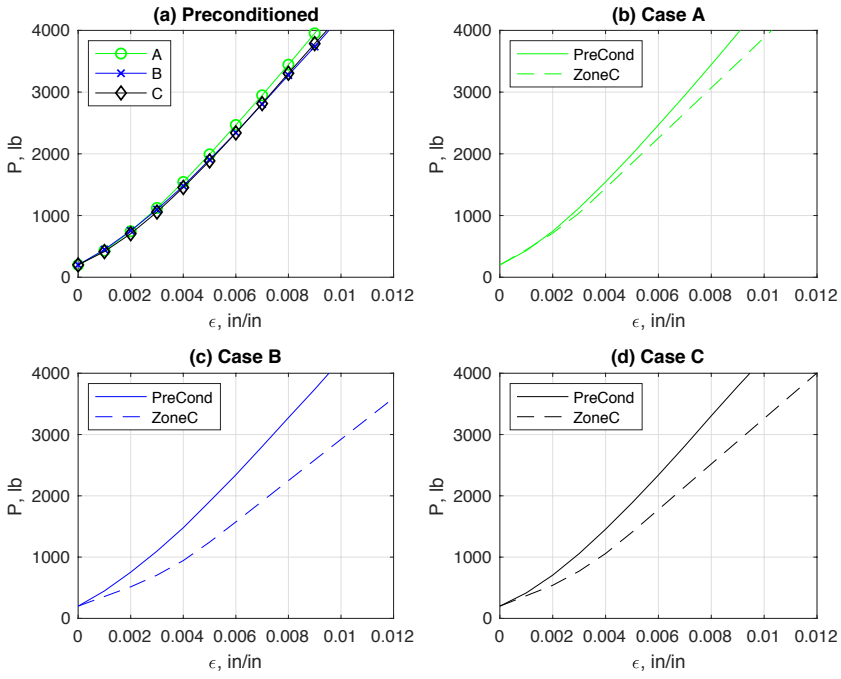

Figure 21. Comparison of hoop webbing average load-strain curves.

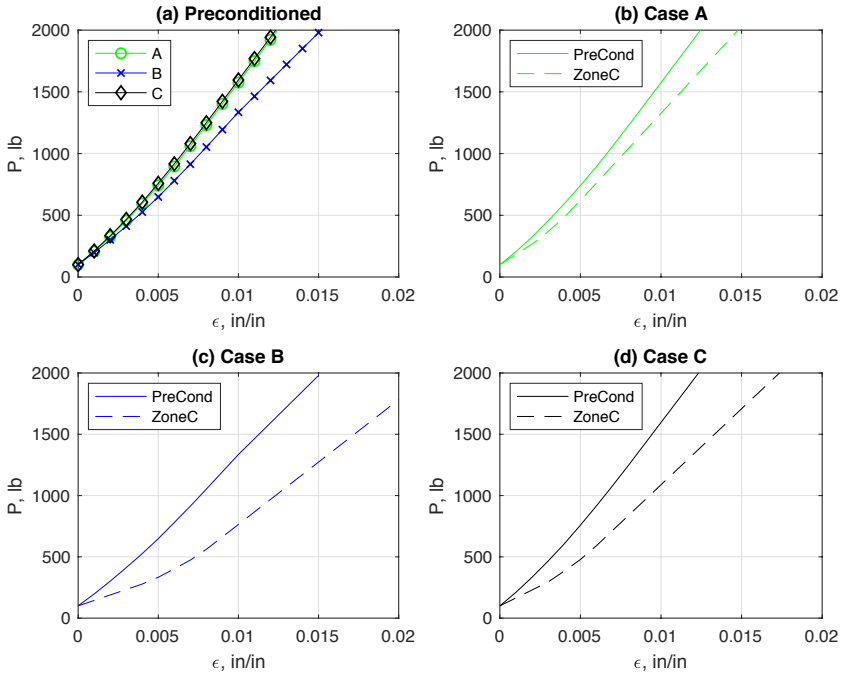

Figure 22. Comparison of axial webbing average load-strain curves.

Appendix A

Comprehensive history plots are provided for Cases A (Dec), B (May) and D (Aug). These plots complement the data provided in Figures 8 through 13 for Case C of the main report. As for the figures contained in the main text, anomalous histories have been identified.

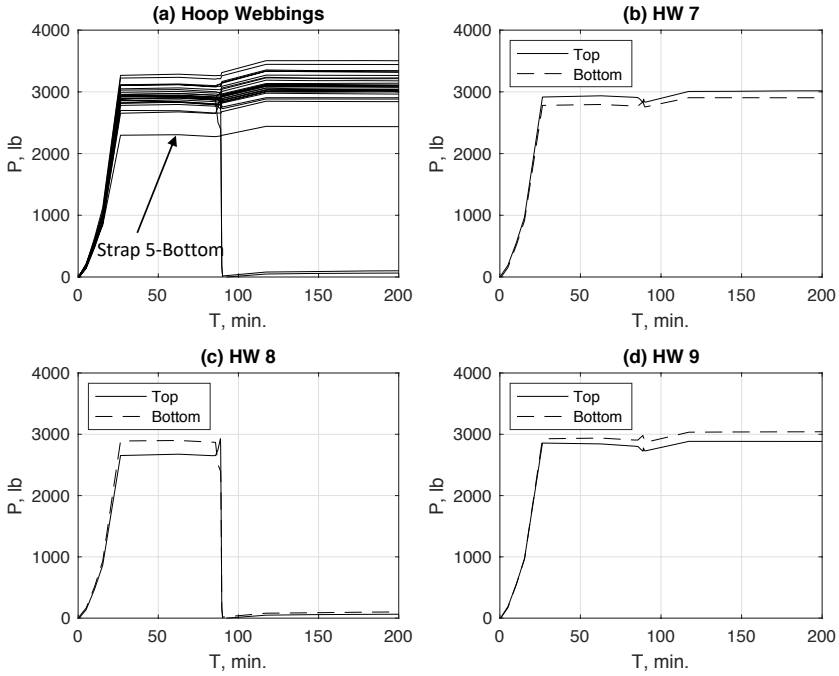

Figure A-1. Load histories for hoop straps [Case A].

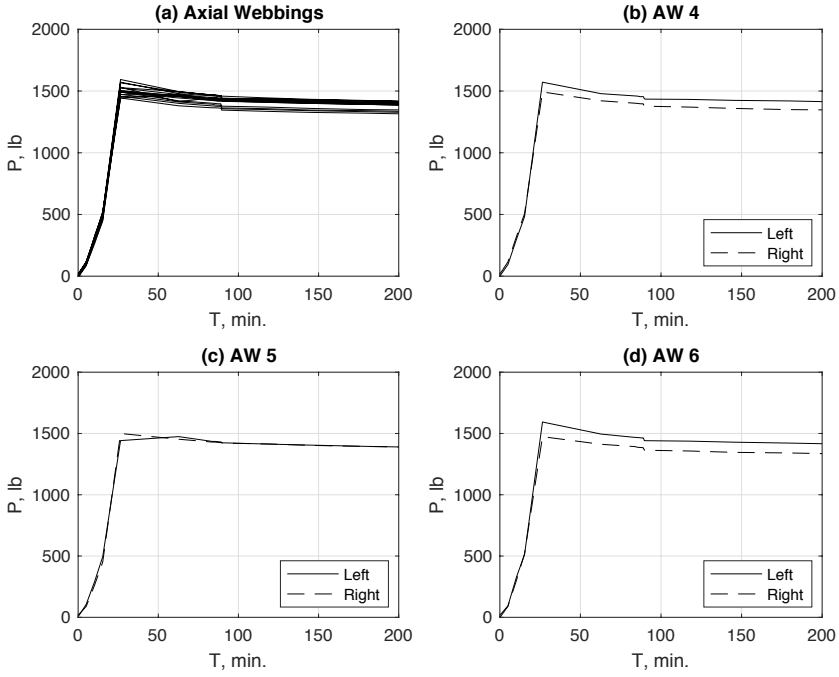

Figure A-2. Load histories for axial straps [Case A].

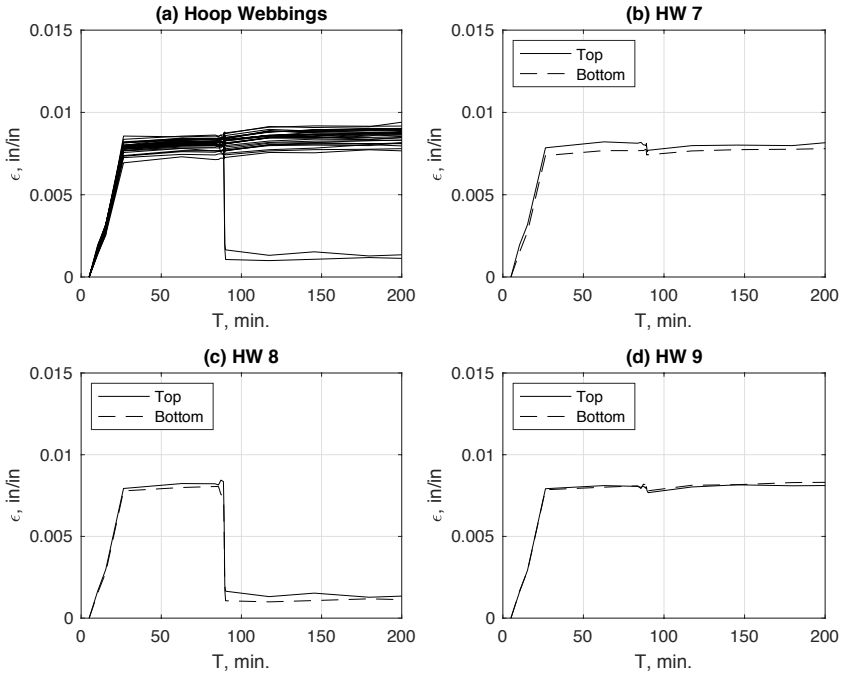

Figure A-3. Zone-C strain histories for hoop straps [Case A].

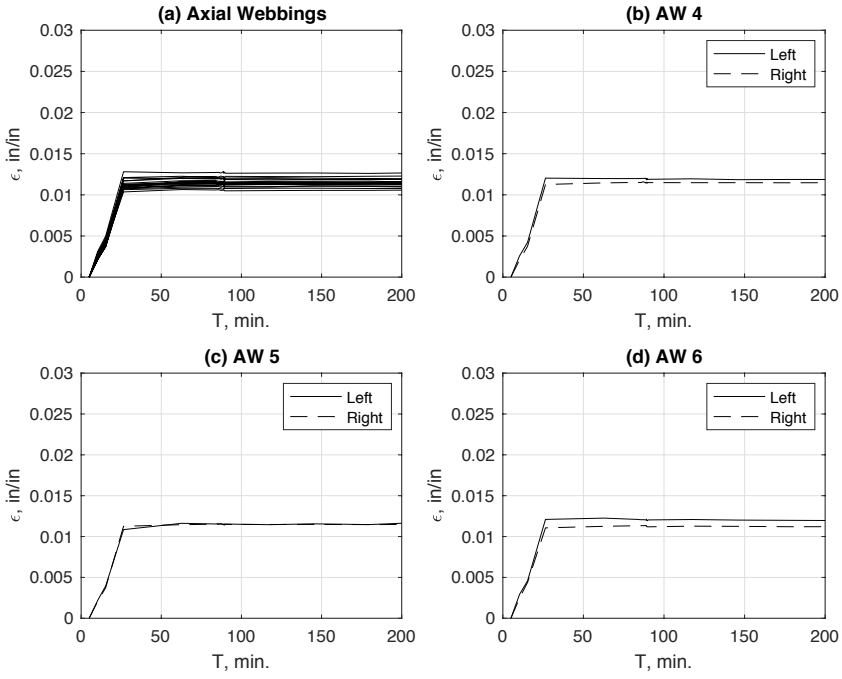

Figure A-4. Zone-C strain histories for axial straps [Case A].

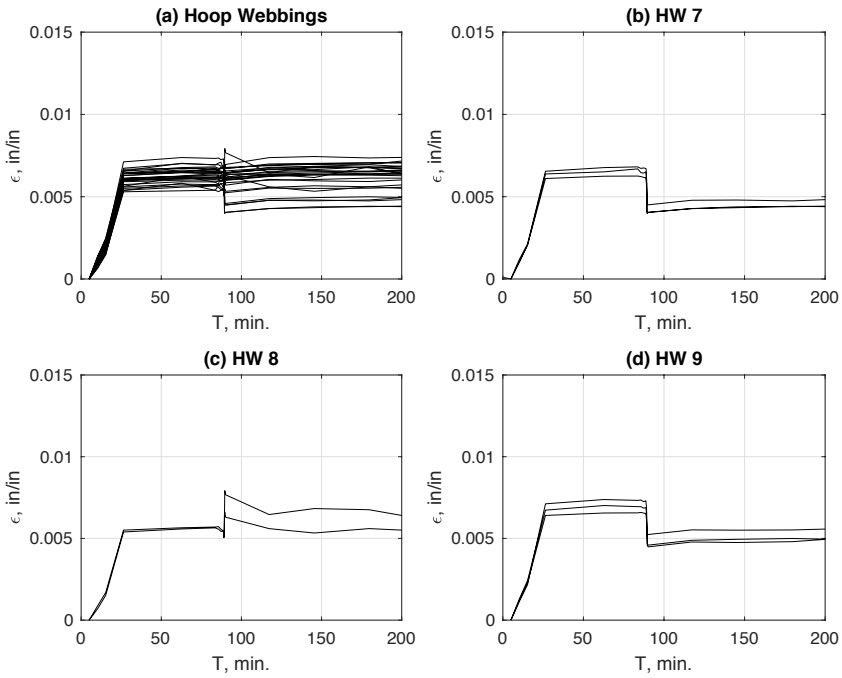

Figure A-5. Zone-A strain histories for hoop straps [Case A].

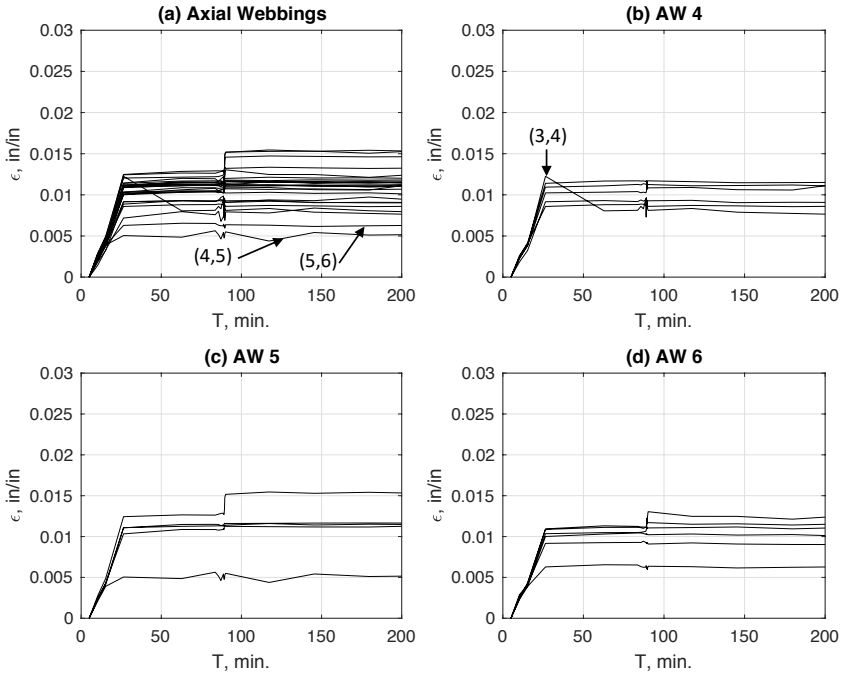

Figure A-6. Zone-A strain histories for axial straps [Case A].

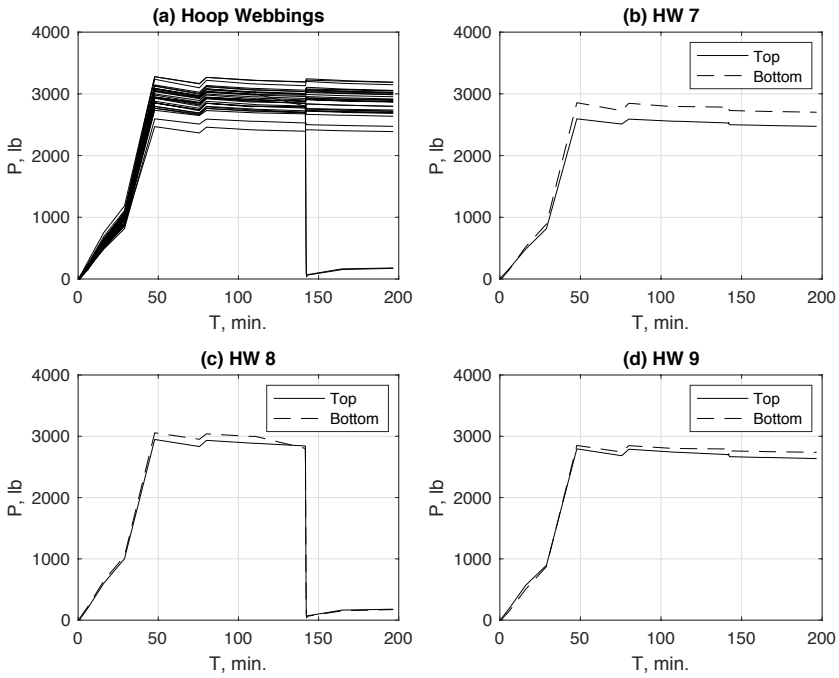

Figure A-7. Load histories for hoop straps [Case B].

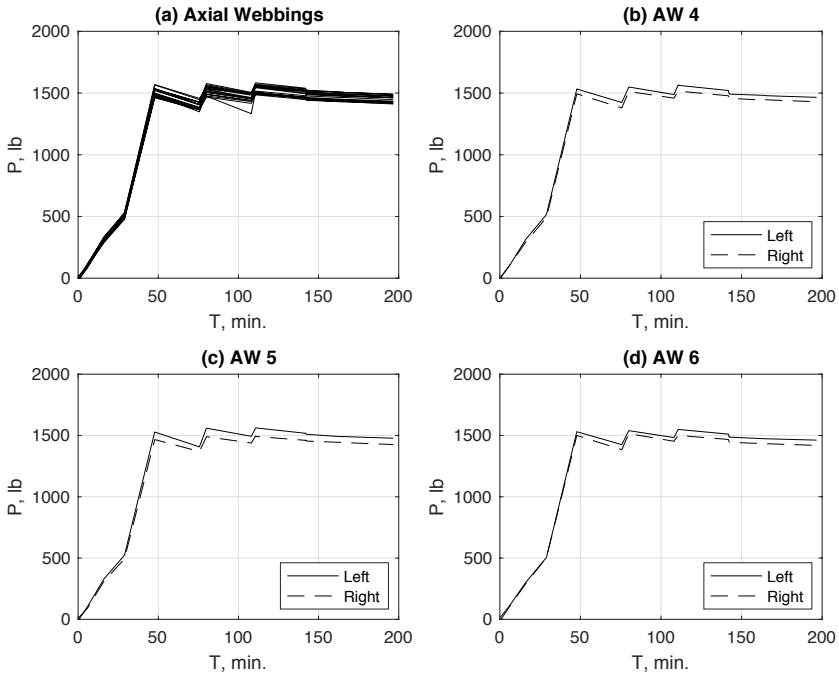

Figure A-8. Load histories for axial straps [Case B].

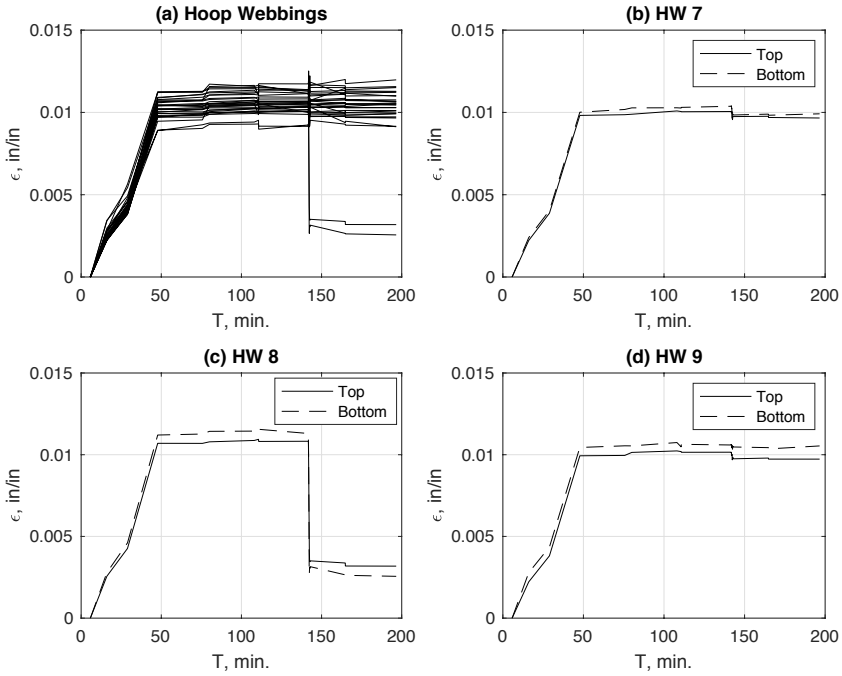

Figure A-9. Zone-C strain histories for hoop straps [Case B].

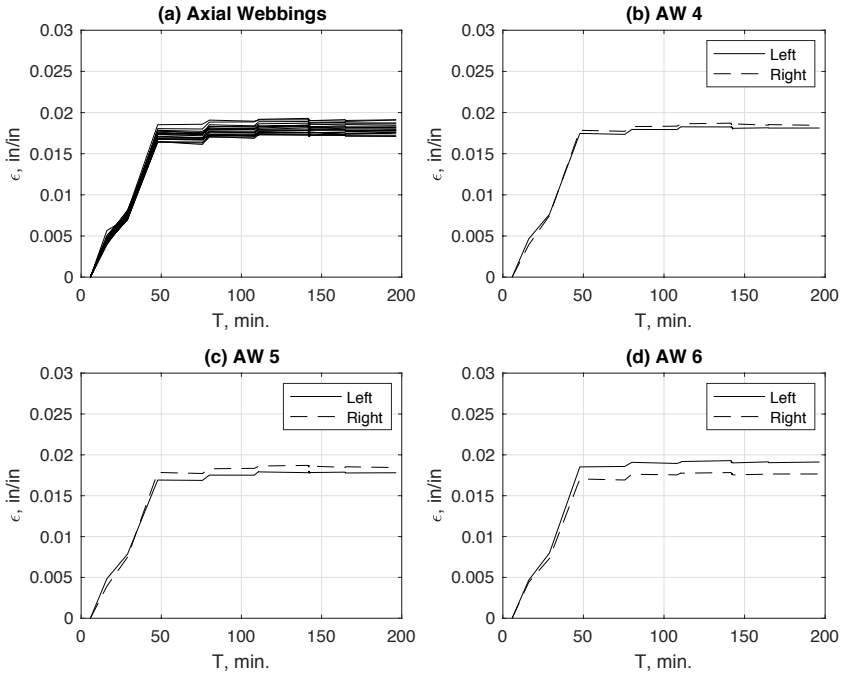

Figure A-10. Zone-C strain histories for axial straps [Case B].

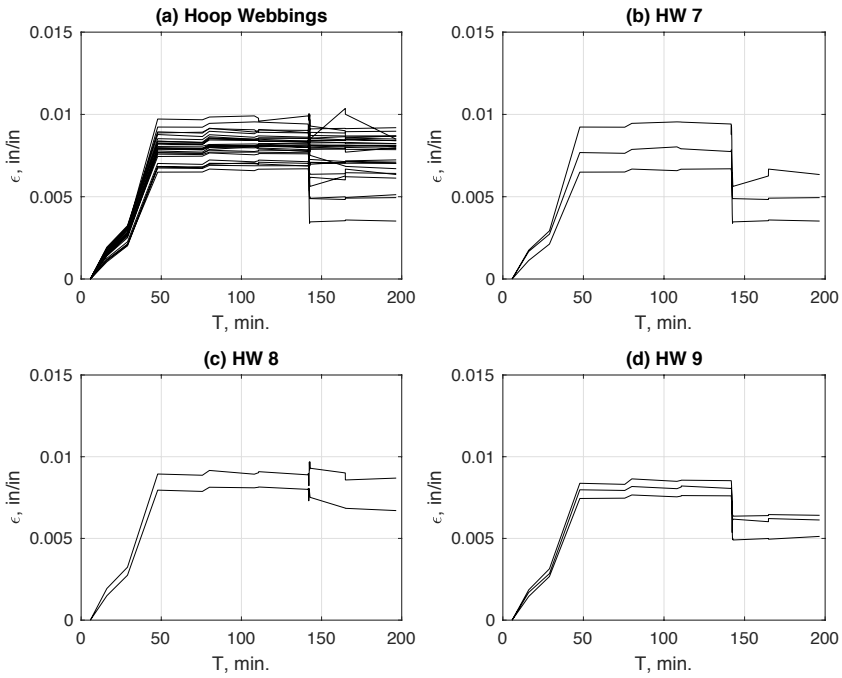

Figure A-11. Zone-A strain histories for hoop straps [Case B].

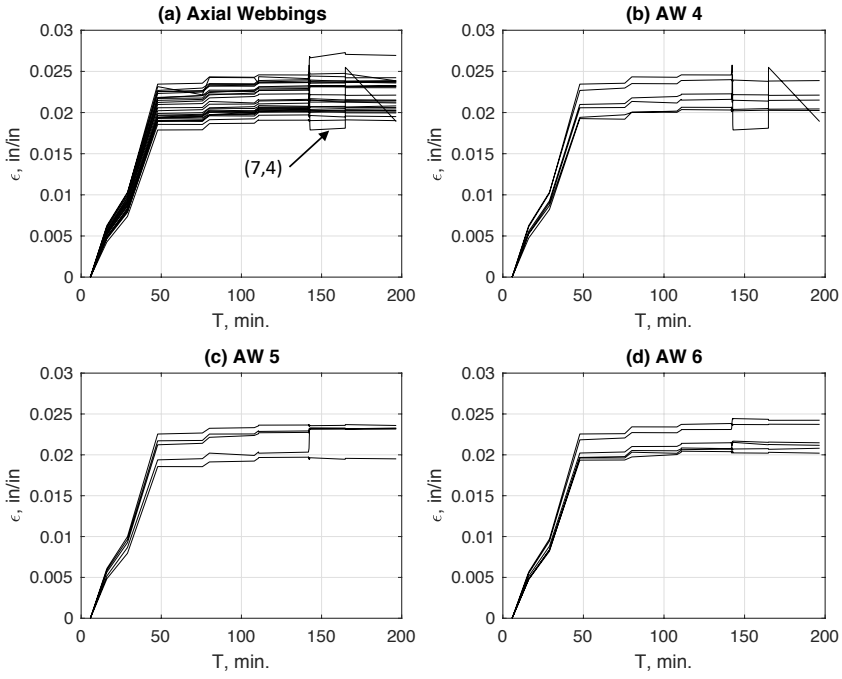

Figure A-12. Zone-A strain histories for hoop straps [Case B].

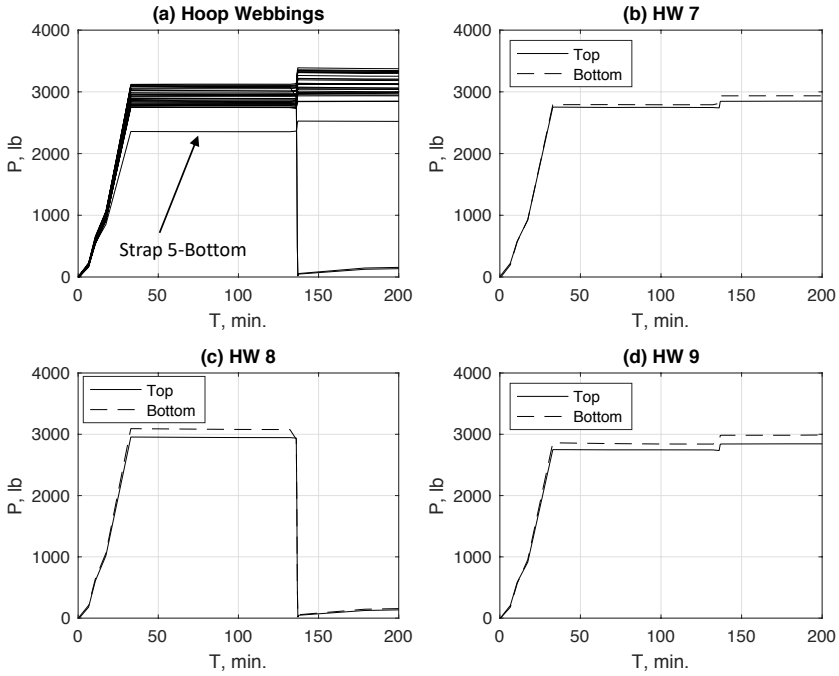

Figure A-13. Load histories for hoop straps [Case D].

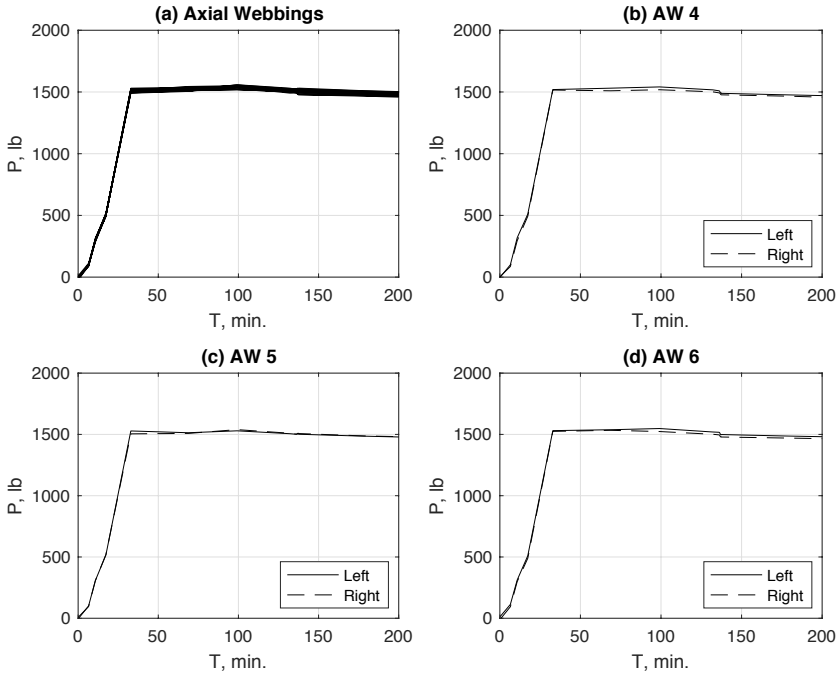

Figure A-14. Load histories for axial straps [Case D].

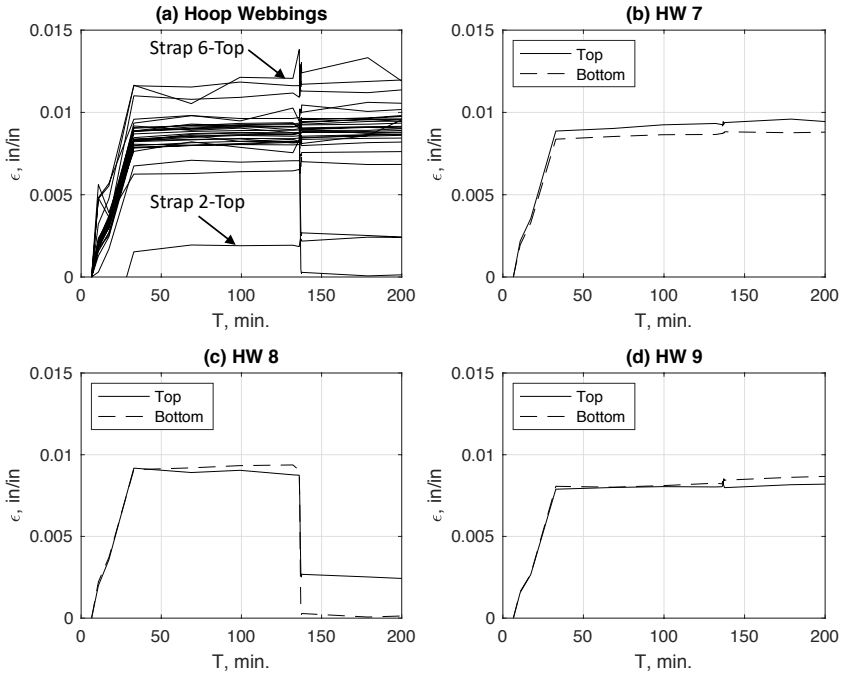

Figure A-15. Zone-C strain histories for hoop straps [Case D].

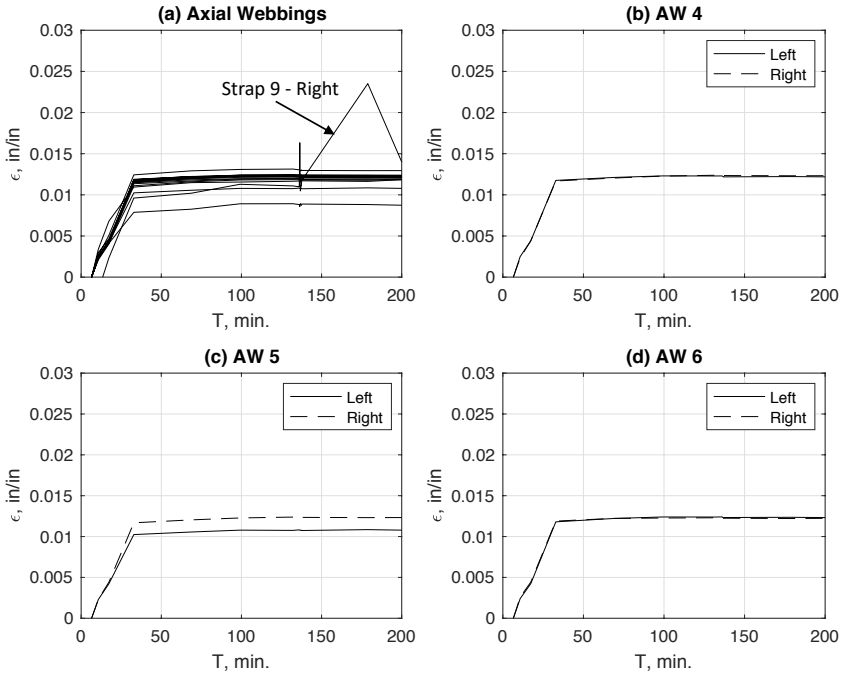

Figure A-16. Zone-C strain histories for axial straps [Case D].

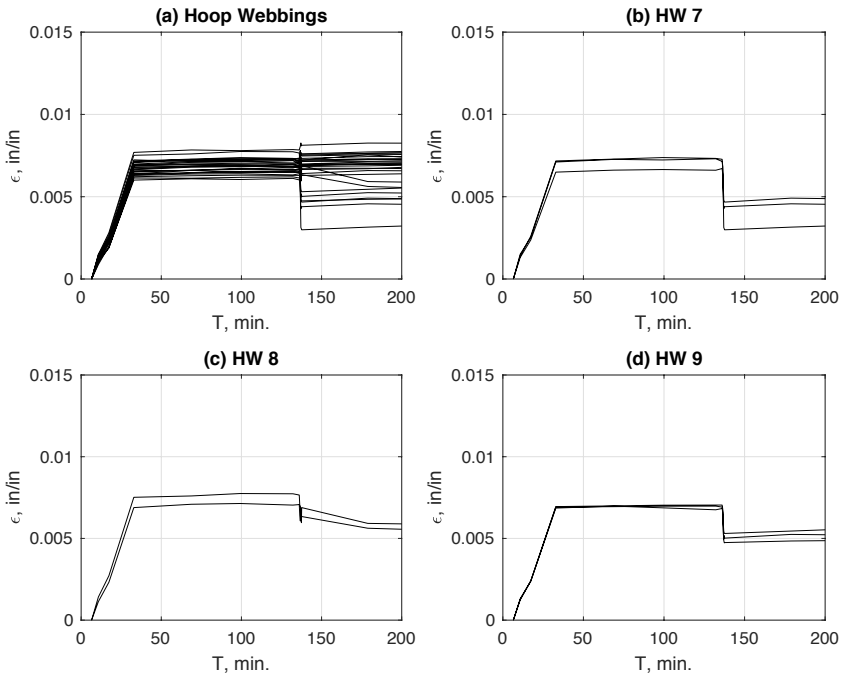

Figure A-17. Zone-A strain histories for hoop straps [Case D].

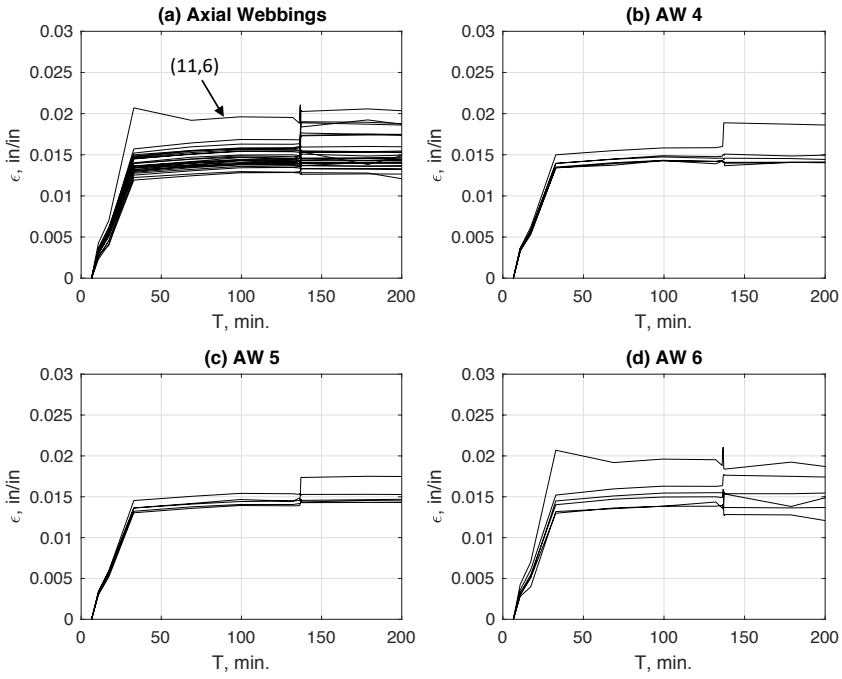

Figure A-18. Zone-A strain histories for hoop straps [Case D].

Appendix B

As noted in the main body of the document, the primary purpose of this study was to understand the detailed load-up and load distribution in a weave of webbings, before and after the loss of tension in one of the webbings. While studying the strain data from the bi-axial test cases, the authors noted that the woven section seemed to behave like a fabric with the webbings acting as large fibers. Thus, the authors considered it noteworthy to provide preliminary results looking at the macro-scale behavior of the webbing weave in this appendix. Preliminary macro-scale results were extracted from the existing data for Cases A through D. However, the spatial trends were similar for all cases, so only figures for Case B will be provided to simplify the presentation. The area of focus is Zone A, as noted in Figure B-1, as well as for a smaller region within Zone A, denoted as Mid3x3. Mid3x3 encompasses the area where HW 7-9 and AH 4-6 cross at the center of the weave. In this appendix, strain color contour results will be presented. These results provide global insight about strain gradients and range in magnitudes of the strains. These strain contour results are accompanied with load-strain graphs where the strains were computed by averaging over Zone A or Mid3x3 for the in-situ bi-axial loading. These types of data could inform macro-scale model development, where the webbing concept for an entire habitat could be represented by using bi-axial material properties, rather than individual webbings.

The full-field strain results are impacted by a number of quantities, including (*where the related VIC-3D terminology is provided in italics*): the size/density of the speckle pattern in conjunction with the camera/lens specifications (determines the *subset size*); the requested overlap of subsets (or *step size*); the quality of the digital images (affects the *noise level*); and the strain spatial smoothing parameter (or *filter size*). Although the VIC-3D terminology has been provided, other commercial full-field photogrammetry DIC systems will likely have similar parameters. For the results provided here, the digital images were read into the DIC system and computations were executed using the recommendations provided by the DIC system. Specifically, for these figures the *subset size* is 51 pixels (approx. 0.5 inches), the *step size* is 7 pixels (approx. 0.07 in), the *noise level* is 8, and the *filter size* is 15. In other words, an area of 51 x 51 pixels is used to estimate the displacement of a node at the center of the subset from its initial location. Each node with an accompanying subset area is spaced 7 pixels apart, therefore the same pixels will appear in multiple subsets. The DIC user's manual indicates that a noise level of 8 is usually acceptable for most applications. Once all of the subset displacements have been determined, the strains are computed. The filter size impacts how large of an area is used in a weighted average to spatially smooth the inherently noisy strain results. The speckle pattern was applied to the webbings to enable detailed strains for each webbing.

Strain color contour results are provided in Figures B-2 through B-5. The strain ε_{xx} is aligned with the axial webbings, while ε_{yy} is aligned with the hoop webbings. For Figure B-2 and

B-3, the strains were acquired at SP4, while Figures B-4 and B-5 contain strains at both SP4 and SP5. As a reminder, the webbing loads prescribed for the testing were designed to replicate operational loads of a cylindrical inflatable habitat. These strain data can provide qualitative insights; however, they were not generated from a bi-axial test configuration in which the bi-axial load is the same in both directions.

The charts in Figure B-2 contain contour results for ε_{xx} acquired at SP4. These contour results in Figure B-2(a) highlight the complex strain pattern often exhibited at the micro-scale for a bi-axially loaded weave. Because of this complex pattern, two additional figures have been included that emphasize strain results for either the exposed AW or the exposed HW. Thus, the same data are used in Figure B-2(b), however the strains of the exposed HW are masked such that only the exposed AW results are emphasized. High strain starts near the center of the webbing crossings. Looking at the complementary HW results in Figure B-2(c), where the AW webbings have been masked, the HW show a low ε_{xx} at the webbing crossing center and the strain contours form a diamond pattern emanating from the center. Generally speaking, when a hoop webbing is on top, the ε_{xx} are small or could even be negative. When an axial webbing is on top, the ε_{xx} are high as is expected for strains in the X-direction.

The ε_{yy} contours for loading at SP4 are provided in Figure B-3. There is a distinct difference in the ε_{yy} pattern than observed in Figure B-2 for ε_{xx}. This likely results from the weave configuration. The AW are spaced 0.4" apart, while the HW nearly touch. Thus, there are substantial portions of HW that are not supported by an AW. As was shown for ε_{xx}, complementary figures using the same ε_{yy} data highlight the difference between AW and HW behavior in the y-direction. In Figure B-3(b) for the AW, the ε_{yy} are nearly uniform with small but positive strain values. Next focusing on the HW in Figure B-3(c), large ε_{yy} in an undulating pattern are evident between the axial webbings. This pattern is postulated to result from the load stretching the unsupported portions of the hoop webbings more in these areas where it is not supported and stiffened by the crossing axial webbings.

The impact of release of HW 8 on the strain results are provided in Figures B-4 and B-5 for the x and y directions, respectively. A white dashed rectangle encloses the HW 8 region. At SP 5 on the bottom, one can see that there are several areas between straps where the strains could not be processed. This likely results for those areas due to the change in the tracked subset area being significant enough that a correlation between images couldn't be found. As a check on the results provided in the main body of the report, AW (8,5) has been highlighted at SP4, the area strain increases, which corresponds to the results shown in Figure 17. On the other hand, for the y-direction strains in Figure B-5, the strains on HW 8 change substantially in the area between the axial webbings. A visual inspection of the strain contour results of Figures B-4 and B-5 seem to confirm that the release of a webbing causes local but not global changes.

Finally, the strains averaged over Zone A and Mid3x3 were plotted versus the set points in Figure B-6. As the load in the two directions was not the same, it is not appropriate to consider

the data as input for a bi-axial fabric material model. The top two graphs provide the raw strains, while in the bottom two graphs the strains are normalized to the value at SP1, as was done for the strains in the main body of the report. The solid lines are the strains averaged over Zone A, while the strains averaged over Mid3x3 are represented by dashed lines.

These are initial results that demonstrate the complexities of analyzing a bi-axial webbing weave and the need to study and compare the full-field results with the individual webbings and cross-over points given the observed behavior of the webbings in between the crossovers. Future tests will include study of the macro behavior of the weave in comparison to the micro, or single webbing, behavior to find optimal approaches to modeling a large inflated structure.

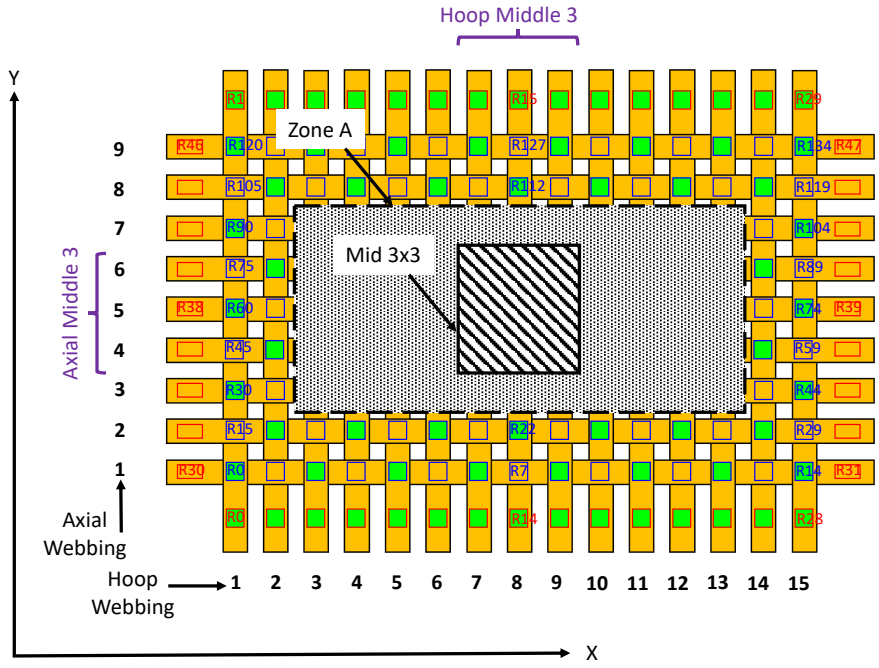

Figure B-1. Schematic of woven-webbing component (not to scale).

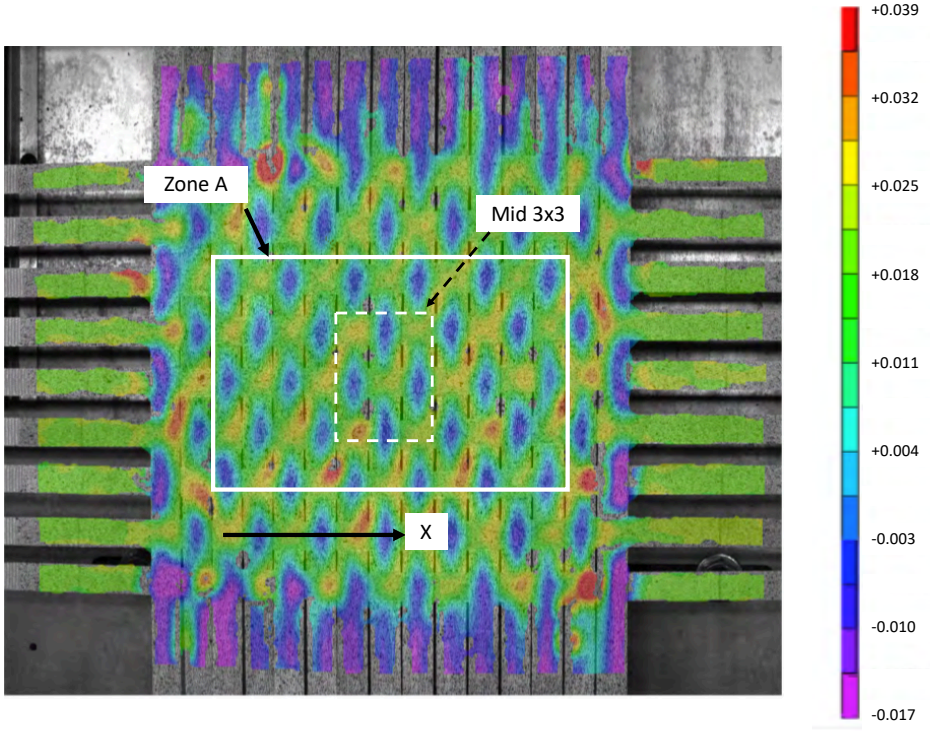

(a) Full-field results.

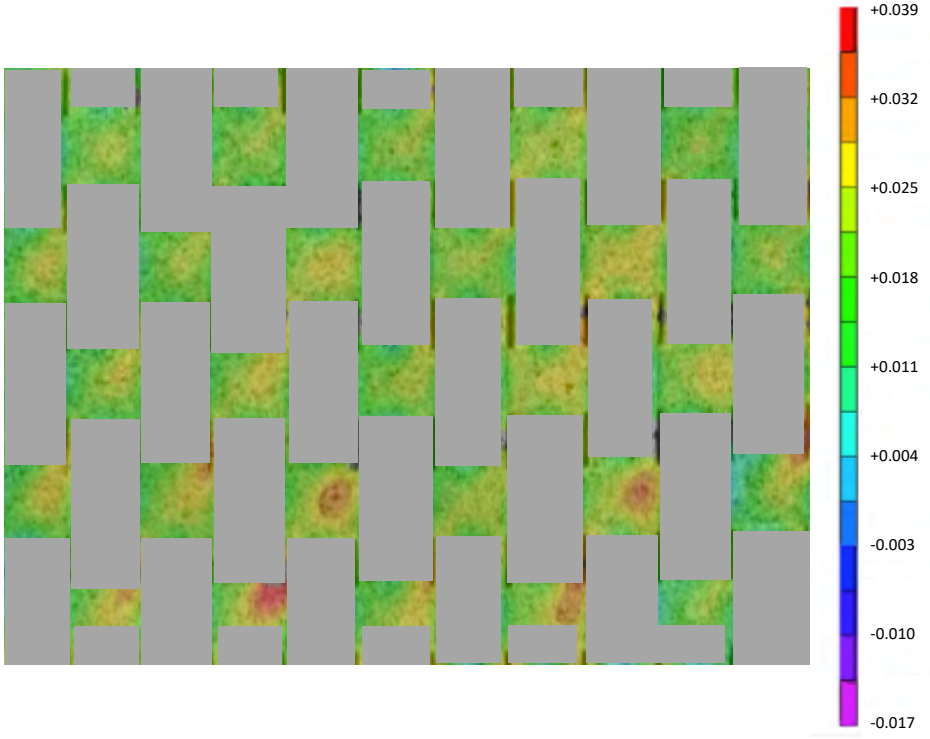

(b) Zone A with HW masked.

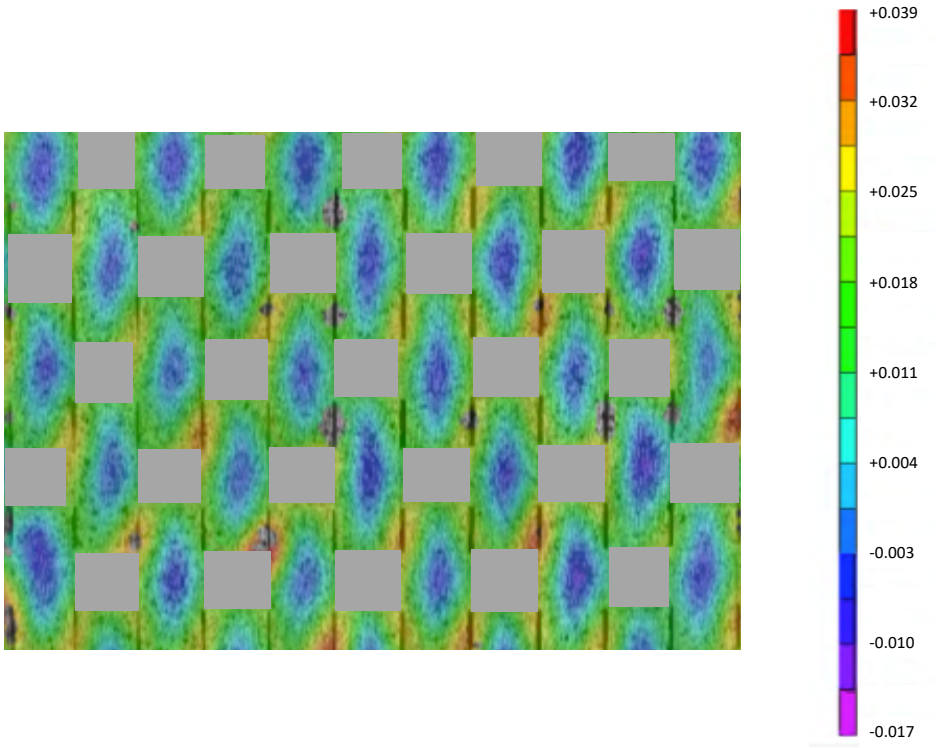

(c) Zone A with AX masked.

Figure B-2. ε_{xx} results at SP4.

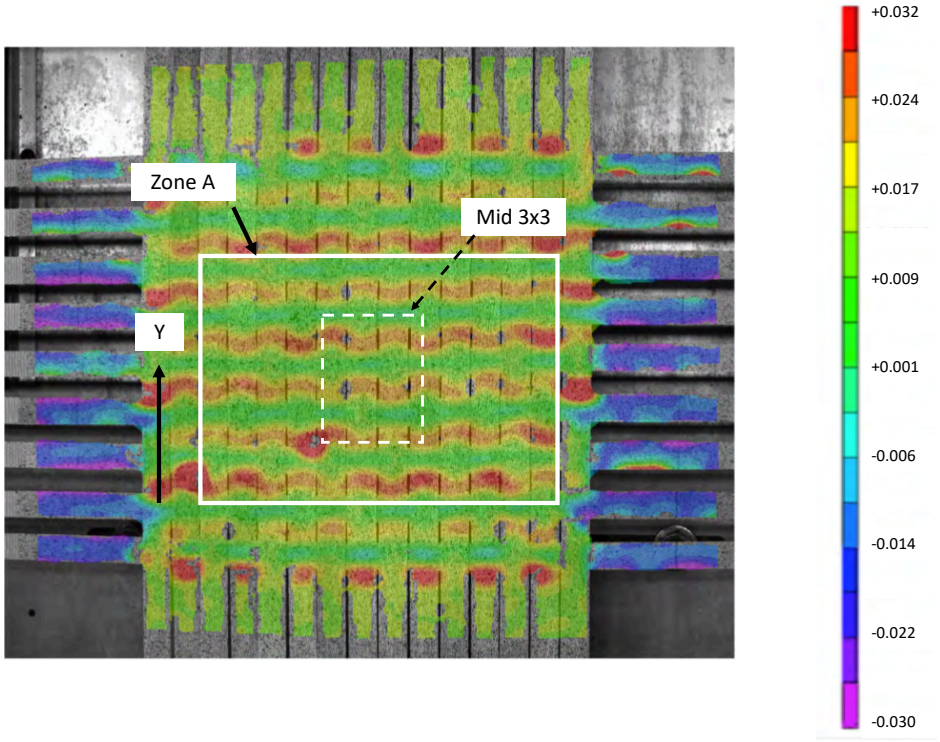

(a) Full-field results.

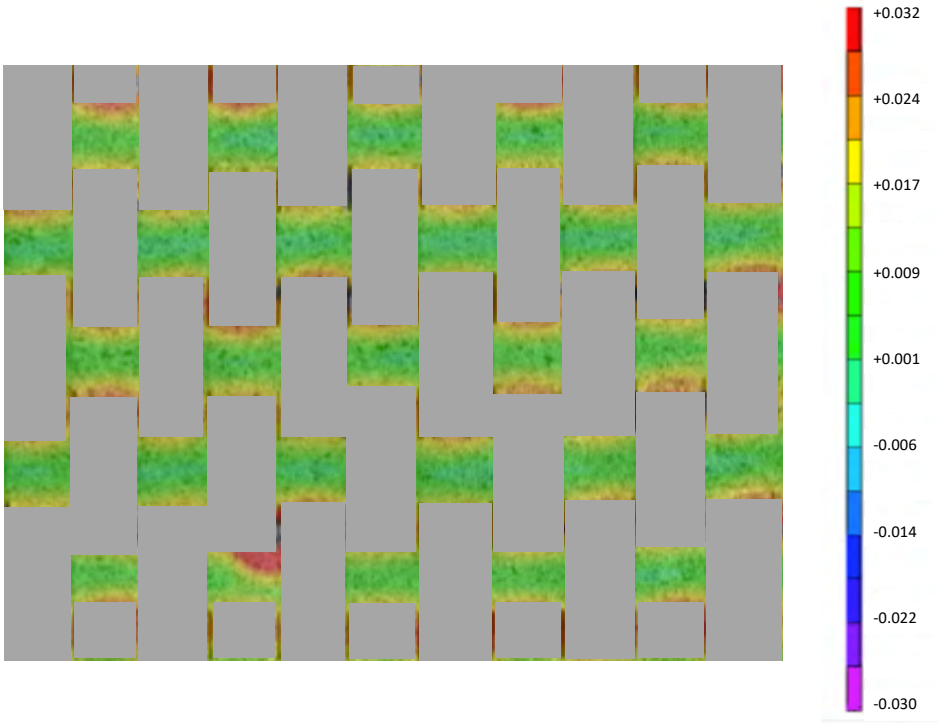

(b) Zone A with HW masked.

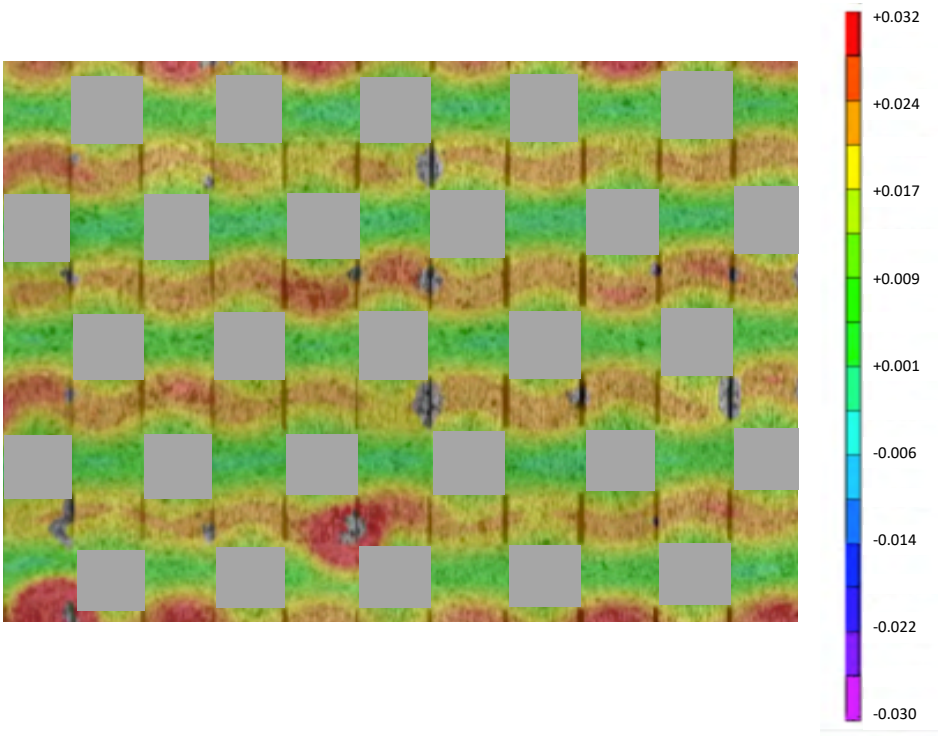

(c) Zone A with AW masked.

Figure B-3. ε_{yy} at SP4.

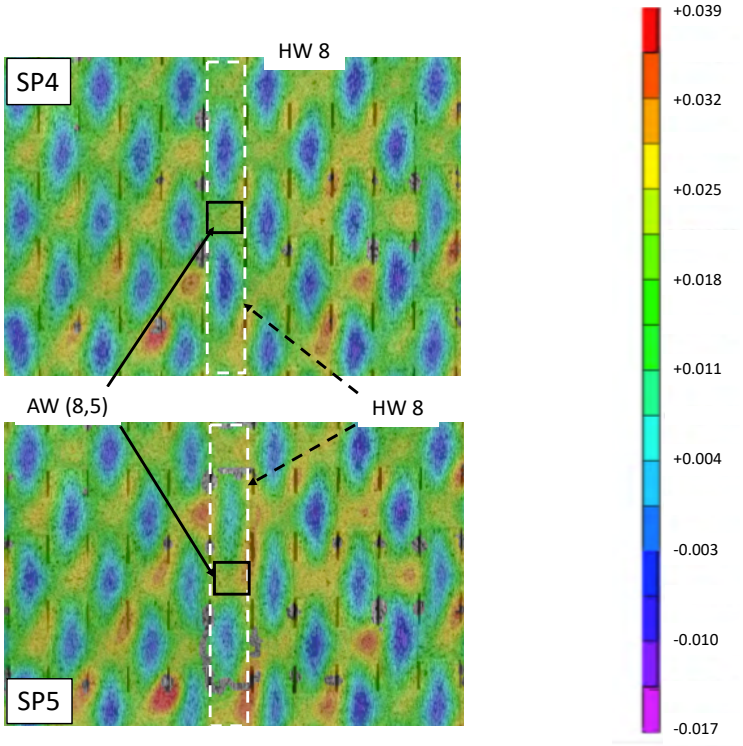

Figure B-4. ε_{xx} in Zone A before and after HW 8 release.

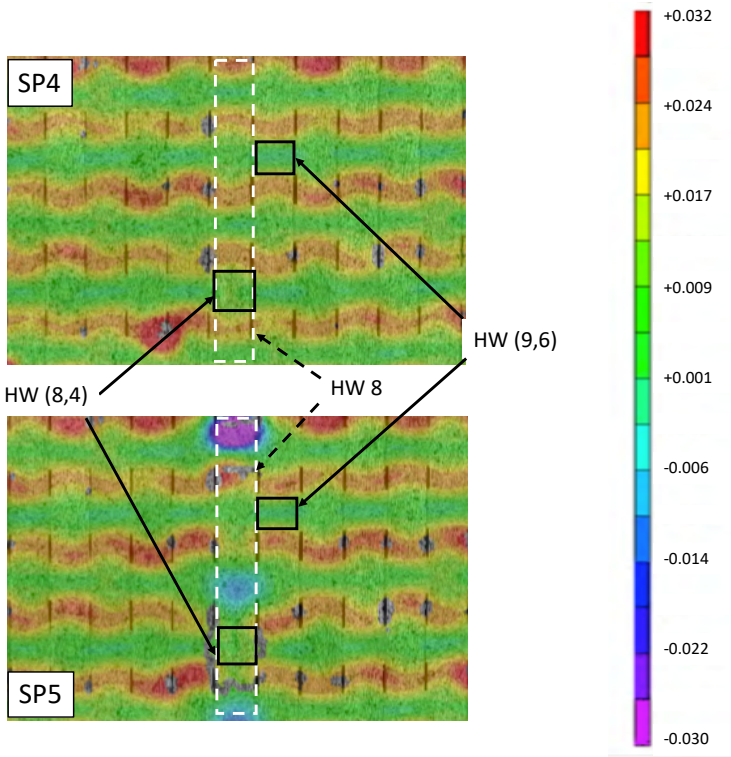

Figure B-5. ε_{yy} in Zone A before and after HW 8 release.

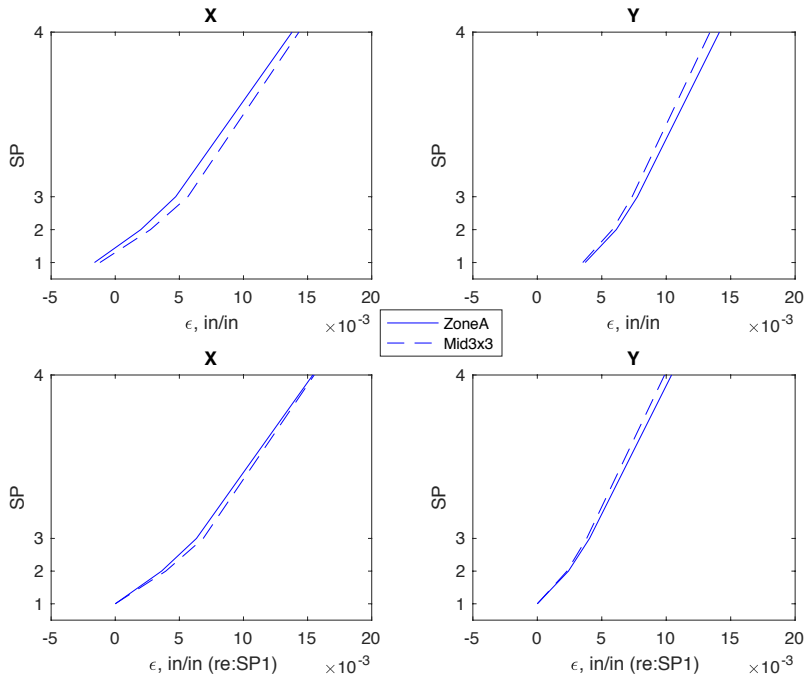

Figure B-6. Comparison of load-strain curves from in-situ bi-axial load testing.

Appendix C

This section describes a complementary activity that studied the ability of surface-mounted accelerometers on the woven-webbing panel described in the main report to measure the propagation of a structural event. For this reason, the area tested was well-removed from the frame, enabling the capture of the initial pulse propagation. The ability to measure these events can influence evaluations of both passive and active structural health monitoring approaches. The primary purpose of this testing was: to understand the physics underlying the propagation responses; to identify areas for improvement; and to assess the appropriateness of the instrumentation approach.

A schematic of the test setup with instrumentation locations is provided in Figure C-1. The 7 accelerometer locations are denoted by red text with annotation “A”, while the hammer tap locations are denoted by blue text with annotation “H”. The table column specifying “Webbing Surface” indicates whether the accelerometer or hammer is directly contacting a hoop webbing or an axial webbing. The accelerometers are placed on both hoop and axial webbings using double-sided tape; however, the hammer is directly impacting only an axial webbing for this set of results. Previous testing showed that whether the hammer tapped on a hoop webbing or an axial webbing did not influence the vibration propagation. The accelerometers were PCB StructCells type 330B, with a nominal sensitivity of 100 mV/g. The frequency range was specified by the manufacturer as 2 to 1,000 Hz, however calibration testing of the accelerometers showed that they were within ± 3 dB up to 4,000 Hz. The data was not filtered prior to digitization. The analog-to-digital conversion was performed using a National Instruments USB-6003, which has an input capability of up to 8 channels and a maximum aggregate digitization rate of 100,000 samples-per-second.

As the tap testing was performed manually, the amplitude of the loads varied from tap to tap. Therefore, to support the evaluations of the repeatability and consistency of the instrumentation and structural responses, the acceleration traces were normalized by the corresponding peak of the tap load. For each hammer location, the time-averaged responses were based on a nominal 10-tap sample. Occasionally a hammer pulse was so low that the transducers could not track the response. In these cases, the pulse was omitted from the averaging process. As experience was gained with the manual tapping, the frequency of these low magnitude taps decreased.

Preliminary testing was conducted with a PCB type 086B01 impact hammer. The normalized accelerations used to evaluate the repeatability and symmetry of the woven-webbing structure responses are provided in Figures C-2 through C-4. For the data acquired for these figures, each of the data channels was sampled at 10 kHz. Representative accelerations are provided in Figure C-2, subplots (a) through (c), with the instrumentation layout provided in subplot (d). In this case the tap hammer provides an excitation at location H_C. The accelerometer locations (A_1, A_5, and A_7) were selected for presentation as they will be the focus of subsequent testing. The acceleration history results show that when repetitively tapping the structure 10 times consecutively, the normalized accelerations of the sample are acceptably repeatable. The repeatability assessment is dependent not only on consecutive taps, but also on nonconsecutive taps. Hence, the 10-tap samples were repeated, such that a 10-tap sample was acquired for each

hammer location, H_A through H_C; then, a 10-tap sample at each of the 3 hammer locations was again acquired. The averaging of the 10-tap sample was performed in the time domain, see Figures C-3(a) through (c). The nonconsecutive repeatability is good with regard to the relative magnitude and phasing. To help in understanding the uniformity of the webbing weave, averaged histories for responses at paired locations are provided in Figure C-4, subplots (a) through (c). The responses at symmetric locations (A_1 vs A_4, A_2 vs A_5, and A_3 vs A_6) are nearly indistinguishable. In summary: 1) the propagation from hammer taps on the weave are repeatable such that the time-averaged responses will be used in the subsequent assessments; and 2) acquisition of data at each of the 7 locations was not required to assess responses as demonstrated by the symmetry assessment.

Following the preliminary testing, it was decided that a higher data acquisition rate was needed to adequately capture the initial vibration propagation. To accommodate the higher acquisition rate, the number of accelerometer locations was reduced to three, specifically A_1, A_5, and A_7, while the per-channel data acquisition rate was increased to 25 kHz. In addition, the excitation hammer was also changed to a micro-hammer (PCB type 086E80) typically used to test electronic boards, with a nominal sensitivity of 100 mV/lb_f. One reason to use this hammer was to understand the ability of the instrumentation to capture low level events. For reference, the measured impulse of the taps ranged from 0.013 to 0.026 lb_f-s. For samples acquired using the micro-hammer, there were no issues with any of the responses as too low to track.

The effect of webbing load on the averaged acceleration histories are provided in Figures C-5 through C-7, with each figure corresponding to one of the hammer tap locations. The time axis has been extended for these plots to capture the propagation for samples acquired at SP1. First, focusing on the responses for taps at location H_A near accelerometer A_1 (Figure C-5), as the tension is increased, the time-of-arrival decreases, the initial pulse amplitude decreases, while the second pulse amplitude increases. For tap location H_B (Figure C-6), the time-of-arrival is shorter for accelerometer A_5 and similar timing for both A_1 and A_7. Taps at location H_C are again closer to accelerometer A_1, which is evident in the shorter time-of-arrival. Little difference is seen in the time-of-arrival between A_5 and A_7.

Next the impacts on the acceleration responses resulting from the loss of the load on HW 8 are provided in Figure C-8 through C-10 for the 3 tap locations. Similar trends are seen for taps at locations H_A and H_B, Figures C-8 and C-9 respectively. Once HW 8 is released, the accelerations at A_1 and A_5 change slightly. On the other hand, the change in response at A_7 is pronounced. (It should be remembered that accelerometer A_7 is on AW 9 where is crossed over HW 8.) Specifically, at SP5 the time-of-arrival is delayed, and the response decreases in magnitude when compared to the responses at SP4. When the hammer taps are on AW 3 where it crosses HW 8, or H_C, the changes are more pronounced for all accelerometer locations, see Figure C-10.

Finally, a series of 5-tap samples along HW 8 were performed at SP5. The corresponding averaged acceleration histories are provided in Figure C-11. In general, the time-of-arrival follows the distance of the taps from accelerometer location. This is most pronounced for location A_7. In addition, the amplitudes of the responses vary inversely to the distance from the tap, with one noticeable exception. The largest response is for taps at location (8,7). Additional testing could confirm the trend or provide additional information about the seemingly anomalous behavior. It should be noted that each of the responses have been normalized to the peak of the hammer tap, so this behavior cannot be attributed to simply hitting the location harder with the hammer.

In summary, these results show that:

- A tensioned, woven-webbing restraint layer will produce repeatable responses when impulsively excited with a hammer tap. In addition, the duplication of the responses at symmetric locations indicates that typical manufacturing tolerances for the woven-webbing configuration may be sufficient to understand the physics of the propagation.
- The data acquisition per-channel rate of 25 kHz is sufficient for this application.
- The increasing webbing loads caused the time-of-arrival to decrease, and the amplitude of the initial pulse to decrease, while the second pulse amplitude increased.
- Releasing HW 8 resulted in:
    - A significant increase in the time of arrival when both the accelerometer and hammer are on a HW 8 crossing location. This is contrary to the surface strain results reported in the main report, which showed little effect on the Zone A strains for HW 8.
    - A small effect on A_1 and A_5 that may be indistinguishable for on-orbit/in-flight.
    - This behavior may also indicate that with the exception of the damaged webbing, the remaining webbings are not generally affected. The responses indicate that the woven-webbing concept may be behaving like a fabric with large fibers.

Again, these tests were conducted to provide data to support both active and passive structural health monitoring technology evaluations. The focus here has been limited to initial propagation of a structural event. Follow-on testing would be needed to sufficiently assess the merits of the approach in this application. Based on these preliminary experiences, future testing should focus on two major areas:

- Accelerometers: Place more accelerometers in Zone A, particularly on the webbing to be released.
- Excitation:
    - For hammer taps: Change to a harder tip on the hammer to extend the higher frequency range for the hammer taps; and incorporate taps with significantly different amplitudes to assess linearity of the responses, etc. The testing for this paper was well below both the hammer load limit and the limit that would damage the webbing.
    - In lieu of normalizing by the amplitude of a hammer tap, additional methods should be evaluated that will produce more repeatable excitation magnitudes.

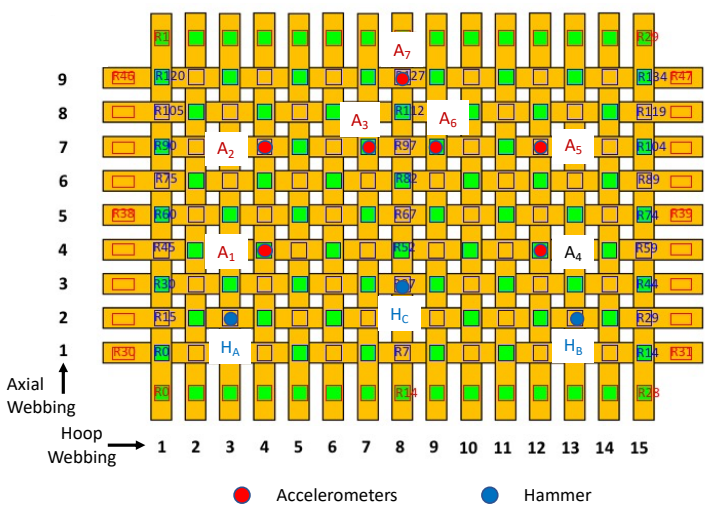

Transducer	Location	Webbing Surface
A_1	(4,4)	Hoop
A_2	(4,7)	Axial
A_3	(7,7)	Hoop
A_4	(12,4)	Hoop
A_5	(12,7)	Axial
A_6	(9,7)	Hoop
A_7	(8,9)	Axial
H_A	(3,2)	Axial
H_B	(13,2)	Axial
H_C	(8,3)	Axial

Figure C-1. Schematic including excitation and responses locations for the tap testing.

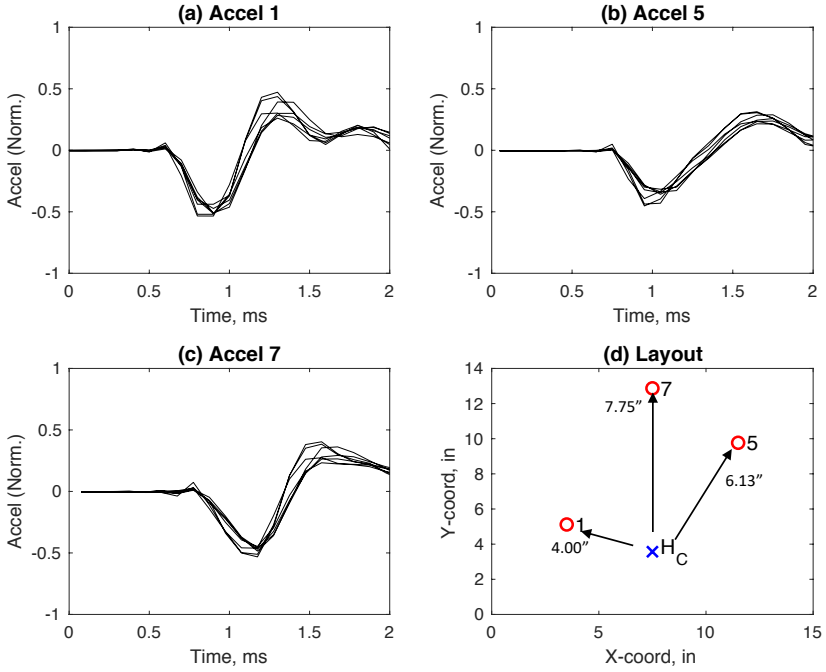

Figure C-2. Acceleration history responses for taps at location H_C.

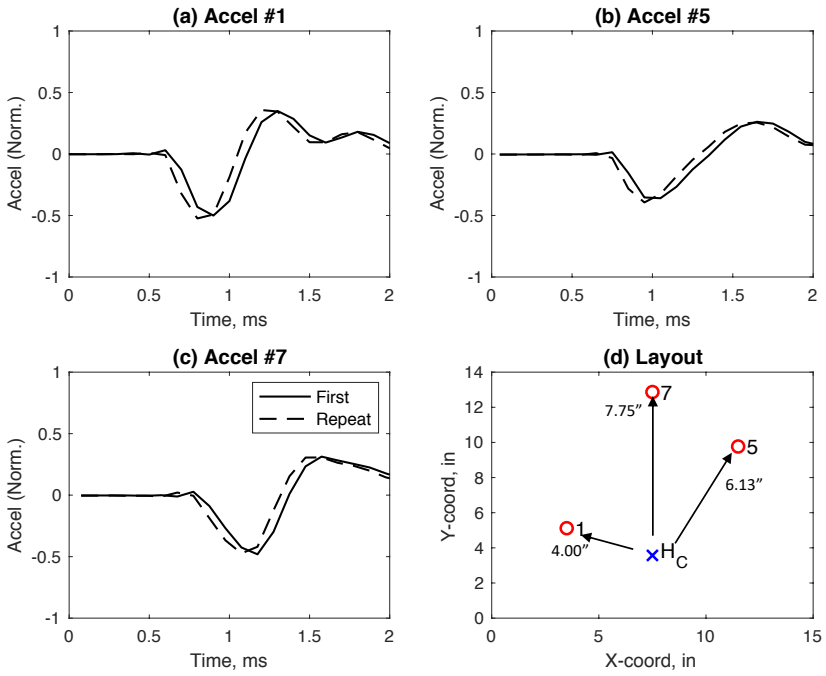

Figure C-3. Comparison of average responses from multiple trials for taps at location H_C.

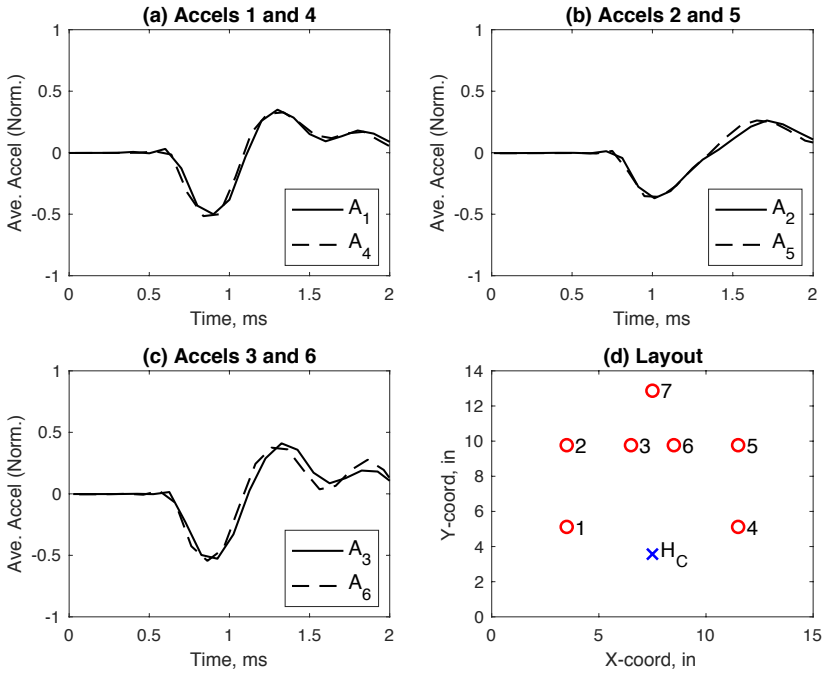

Figure C-4. Comparison of average responses at symmetric locations for taps at location H_C.

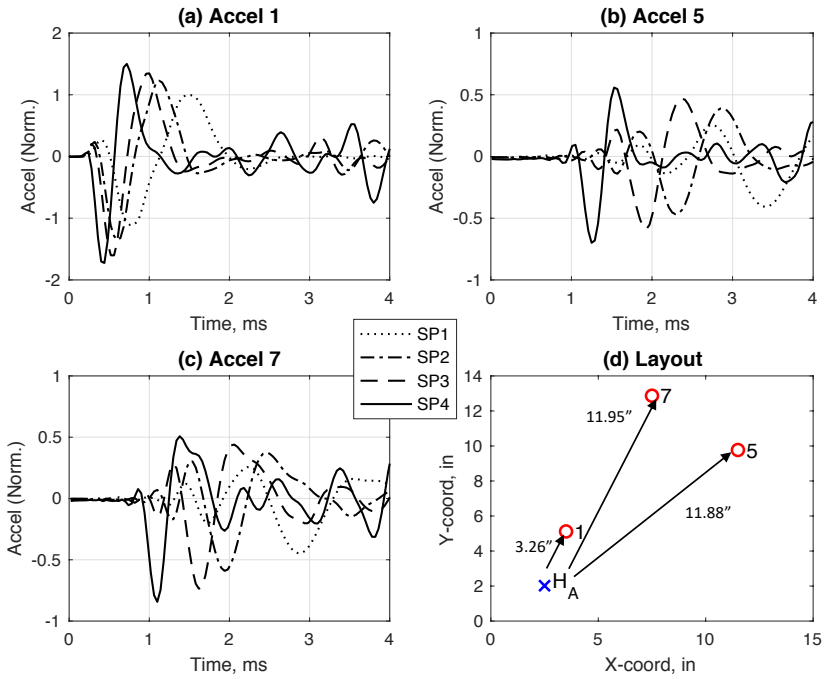

Figure C-5. Effect of increasing webbing loading on average responses for taps at location H_A.

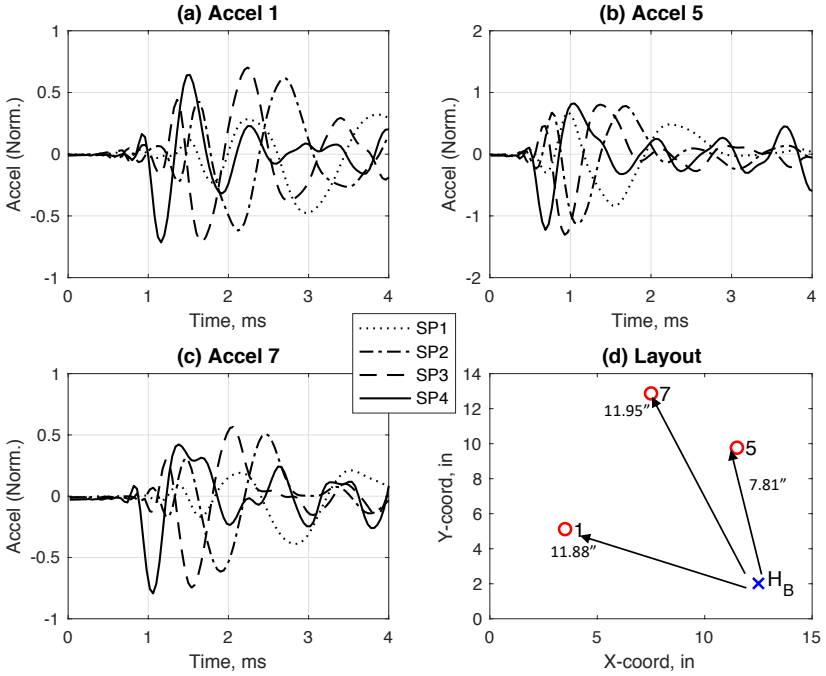

Figure C-6. Effect of increasing webbing loading on average responses for taps at location H_B.

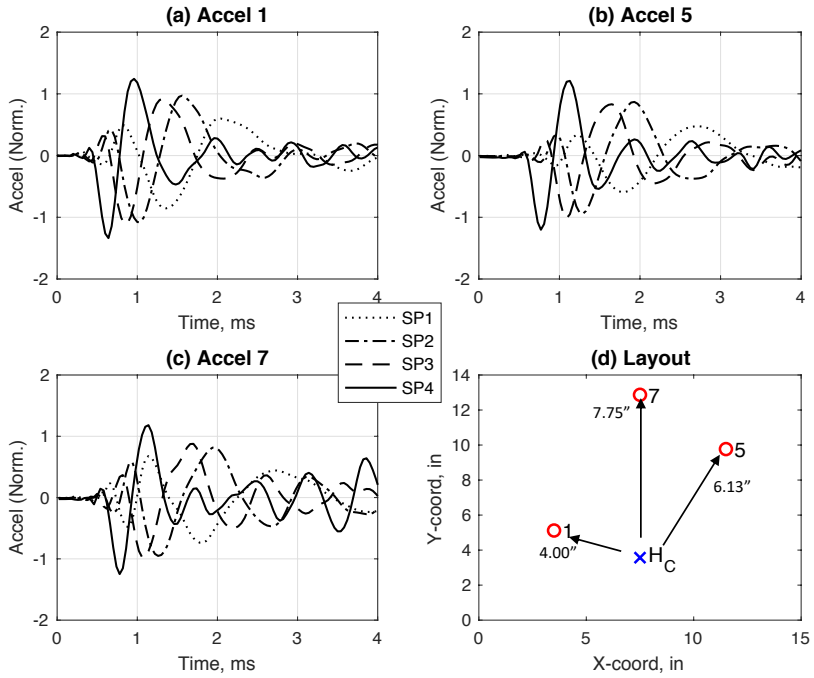

Figure C-7. Effect of increasing webbing loading on average responses for taps at location H_C.

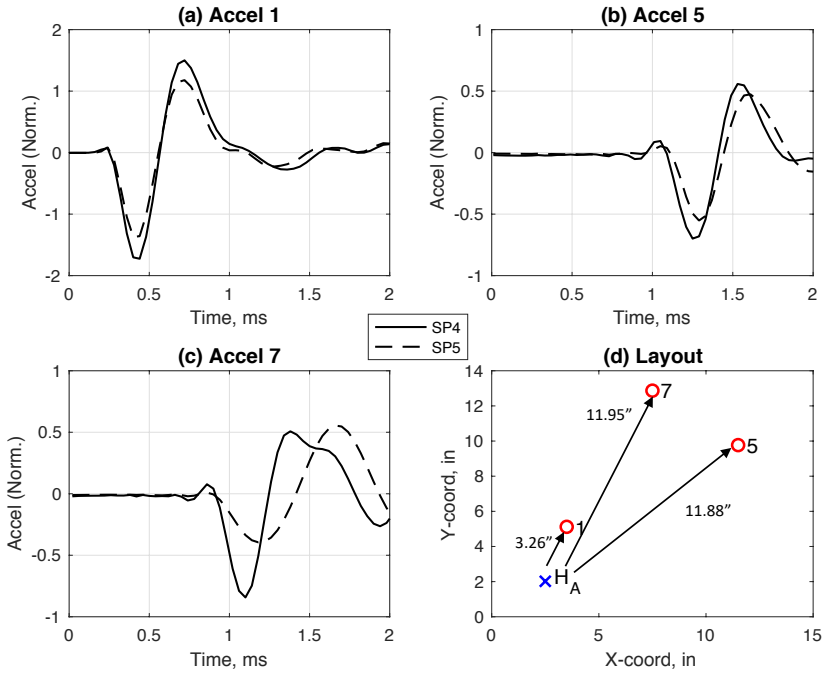

Figure C-8. Effect of HW 8 release on average responses for taps at location H_A.

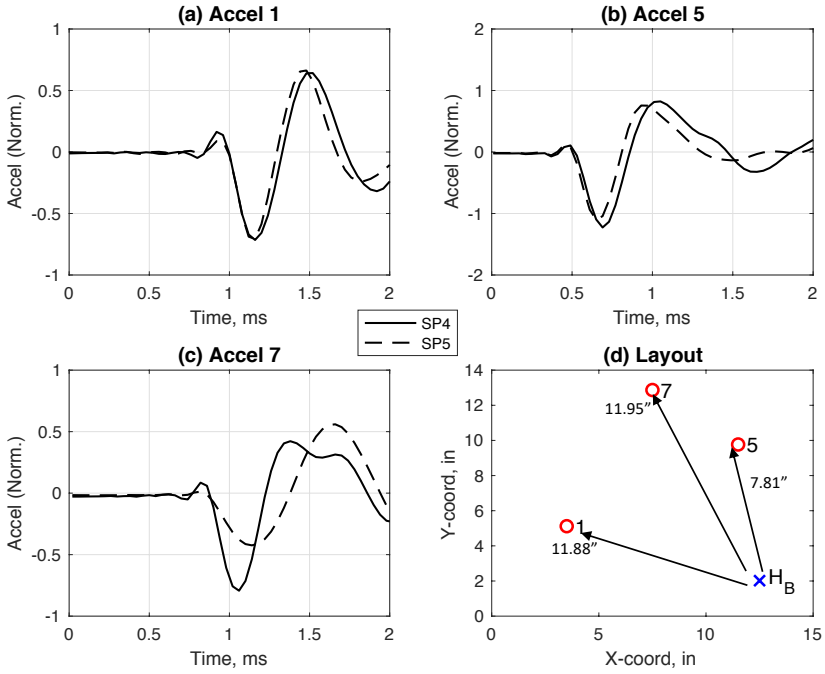

Figure C-9. Effect of HW 8 release on average responses for taps at location H_B.

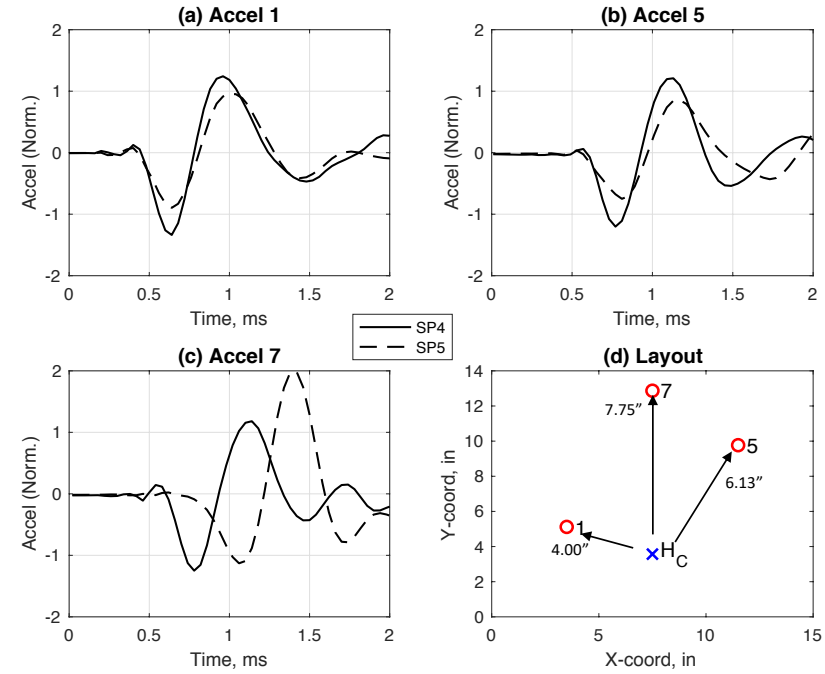

Figure C-10. Effect of HW 8 release on average responses for taps at location H_C.

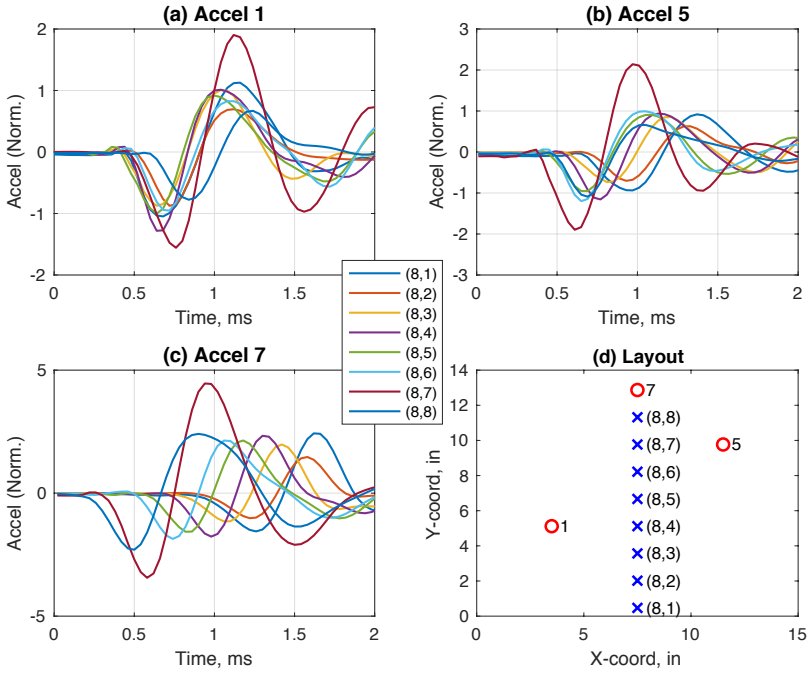

Figure C-11. Average responses after HW 8 release for tap locations on HW 8.

REPORT DOCUMENTATION PAGE

Form Approved
OMB No. 0704-0188

1. REPORT DATE *(DD-MM-YYYY)*	2. REPORT TYPE	3. DATES COVERED *(From - To)*
1-03-2020	Technical Memorandum	

4. TITLE AND SUBTITLE

Bi-Axial Load Testing of a Woven-Webbing Inflatable Space Habitat Restraint Layer Component

5a. CONTRACT NUMBER

5b. GRANT NUMBER

5c. PROGRAM ELEMENT NUMBER

6. AUTHOR(S)

Lyle, Karen H.; Jones, Thomas C.

5d. PROJECT NUMBER

5e. TASK NUMBER

5f. WORK UNIT NUMBER

089407.09.23

7. PERFORMING ORGANIZATION NAME(S) AND ADDRESS(ES)

NASA Langley Research Center
Hampton, VA 23681-2199

8. PERFORMING ORGANIZATION REPORT NUMBER

L-21128

9. SPONSORING/MONITORING AGENCY NAME(S) AND ADDRESS(ES)

National Aeronautics and Space Administration
Washington, DC 20546-0001

10. SPONSOR/MONITOR'S ACRONYM(S)

NASA

11. SPONSOR/MONITOR'S REPORT NUMBER(S)

NASA-TM-2020-220575

12. DISTRIBUTION/AVAILABILITY STATEMENT

Unclassified-
Subject Category 39
Availability: NASA STI Program (757) 864-9658

13. SUPPLEMENTARY NOTES

14. ABSTRACT

This report discusses testing of a bi-axial woven panel consisting of high-strength webbings that represent a portion of the structural restraint layer of an inflatable space structure. Inflatable softgoods vessels are being researched for human space missions as possible habitats, airlocks and tunnel elements. Understanding the complex behavior of the softgoods restraint layer and maturing finite element analysis capabilities to model these structures is critical to their successful implementation. The primary goal of this research is to study the load-up and load distribution in a weave of webbings, before and after the loss of tension in one of the webbings. In addition, a key objective is to evaluate the ability to convert strains measured via photogrammetry using digital image correlation to loads in the weave. The report gives an introduction and objectives for the test program and a description of the test fixture, setup and procedure.

15. SUBJECT TERMS

Inflatable space habitat; load tests; restraint layer

16. SECURITY CLASSIFICATION OF:			17. LIMITATION OF ABSTRACT	18. NUMBER OF PAGES	19a. NAME OF RESPONSIBLE PERSON
a. REPORT	b. ABSTRACT	c. THIS PAGE			STI Help Desk (email: help@sti.nasa.gov)
U	U	U	UU	57	19b. TELEPHONE NUMBER *(Include area code)* (757) 864-9658